N72 33517

REPORT

TO THE

NATIONAL AERONAUTICS AND SPACE ADMINISTRATION

ON

RUBIDIUM^{87} GAS CELL STUDIES

(PHASE I)

NGR 52-133-001

Period covered: April 1, 1970 to April 30, 1972

Quantum Electronics Laboratory
Department of Electrical Engineering
Laval University
Quebec 10, Canada

May 1972

REPORT

TO THE

NATIONAL AERONAUTICS AND SPACE ADMINISTRATION

ON

RUBIDIUM^{87} GAS CELL STUDIES

(PHASE I)

NGR 52-133-001

Period covered : April 1, 1970 to April 30, 1972

Quantum Electronics Laboratory
Department of Electrical Engineering
Laval University
Quebec 10, Canada

May 1972

FOREWORD

This report covers studies made on rubidium gas cells for the National Aeronautics and Space Administration under N.G.R. 52-133-001. The main objectives were the assembly of two rubidium 87 masers out of parts supplied by the National Aeronautics and Space Administration and the determination of the performance of these two masers. These two objectives have been fulfilled entirely. The results obtained are described in this report. Figure 18 is a photograph of the two masers.

The work described here may be considered as a first phase of a more extended program on the development of rubidium masers. The second phase will consist of integrating the maser and its associated electronics into a compact unit that could be used as a stable oscillator. The results reported show that the rubidium 87 maser is the oscillator with the best short term stability when compared to other existing devices.

The studies were done, during the last two years, in the Quantum Electronics Laboratory of Laval University. The scientists who have worked on various aspects of the project are, M. Têtu, G. Missout and G. Busca.

Jacques Vanier, Ph.D.
Associate Professor
(Principal investigator).

Contents

I. INTRODUCTION

Since the realization of the first rubidium^{87} maser operating between the field independent levels at Columbia University[1,2,3], laboratories in private industries and universities have initiated research programs in this field. The interest in the rubidium maser is due mostly to the promise of an unsurpassed short term stability.

Several years have elapsed, however, without any experimental verification of the stability of the masers. Research has been mostly oriented towards the understanding of the basic principles governing the operation of the maser[4]. Furthermore, the rather high stability expected below averaging times of one second, has created a problem in the sense that, for the purpose of comparison, no other oscillators with the required characteristics were available. In fact, it has been found that two similar masers were needed to obtain a short term stability measurement. This is typical of the field of high stability atomic oscillators. A similar situation was encountered with hydrogen masers and its stability was not known until several units were built[5].

The physical construction of rubidium masers may take various forms. The first maser oscillating between the field independent levels consisted of a vacuum tight cavity made of copper plated stainless steel[2]. This type of design permits the realization of a high cavity quality factor, but has the disadvantage of being temperature sensitive. This introduces strong frequency pulling effects. Another approach has been the use of a quartz bulb containor inside a cavity. This arrangement has the disadvantage of reducing substantially the quality factor Q of the cavity. However, it has been possible to design bulbs which are capable of supporting atmospheric pressure, and which

are sufficiently thin to avoid a drastic reduction in cavity Q. We have been able to obtain maser oscillation between the field independent levels with several of these bulbs. Such a construction permits the use of quartz cavities with greater thermal stability than in the case of the stainless steel cavity. It allows also the implementation of external coarse and fine tuning devices as well as variable coupling without interference with the vacuum assembly. We have taken this second approach, for the design of our masers, and we have given it the name "quartz bulb - quartz cavity" approach.

Two of these masers have been built. Their construction has been made essentially out of the parts supplied by the National Aeronautics and Space Administration. In one of these masers, however, another cavity than the one supplied had to be used because of an incompatibility between the storage bulb and the cavity quartz cylinder (the bulb which we needed to use was too large to enter in the cylinder). One of the masers was called NAS 1 and the other, containing the transformed cavity, was called LEQ 1. Both masers have been operating continuously for a period of about six months and extensive measurements of their characteristics have been made.

In the present report, the theory of the maser operation is given in section II and the description of the maser assembly is given in section III. Section IV is devoted entirely to the experimental results obtained. We draw some conclusions on the results obtained and we propose some research projects which seem promising as far as the development of the rubidium maser is concerned.

II. THEORY

The general theory of masers is well known. In fact, as early as 1956, Townes and his colleagues[6] have published the basic theory of the ammonia maser. Thereafter it was only necessary to adapt this theory to the

particular problems or devices that were studied.

The rubidium maser theory follows this rule. However, the method used, to obtain population inversion and the replacement of the original atomic beam by a gas contained in a storage bulb, makes it sufficiently different from the original ammonia maser that a new theory must be developed before any precise conclusions can be drawn on its behaviour. Several attempts have been made in the past in order to obtain a theory describing as closely as possible its operation. These have varied from simple population inversion and energy loss arguments (Davidovits and Novick, 1966)[3] to more exact density matrix calculations (Vanier[4], Alekseyev[7]). We have used this last approach. Recently we have developed it in such a way as to take into account the local variation of the density matrix elements, in the storage container. This theory is described below.

The rubidium^{87} maser: a schematic diagram of the rubidium maser is shown on figure 1. The maser consists essentially of a lamp, a filter, an absorption cell, a high Q cavity and a solenoid to produce the magnetic field. The lamp is made of a large spherical mirror with a pyrex bulb at its focal point. The bulb contains traces of rubidium^{87} and krypton at a pressure of a few torr. The lamp is excited by a r.f. field at a frequency of about 80 MHz. Light from the lamp passes through the rubidium 85 isotopic filter, penetrates inside the cavity and orients the rubidium 87 atoms contained in the storage bulb. The exact functioning of the devices is best explained with the help of figure 2 which is a diagram of the lower energy levels of the rubidium 87 atom. The lamp emits mainly hyperfine lines which correspond to transitions from the P states to the two levels $F = 2$ and $F = 1$ of the ground state. The purpose of the rubidium 85 filter is to re-

move from the spectrum of the lamp the lines corresponding to the transitions from the P state to the level $F=2$ of the ground state. This happens because of the fortunate coincidence of two of the lines of the rubidium 87 and rubidium 85 isotopes. The filtered light penetrates the storage bulb which contains traces of rubidium 87 and nitrogen at a pressure of about 10 torr. The atoms are excited to the P state by the incident light. They are then relaxed to both levels $F=1$ and $F=2$ of the ground state by collisions with nitrogen molecules. Because of the asymmetry in the pumping light a net population unbalance is obtained. When enough atoms are pumped into the upper level $F=2$, and if the cavity has a high Q, self sustained oscillations may be obtained between the $F=2$, $M_f=0$ and $F=1$, $M_f=0$ levels at a frequency of 6.835 GHz.

1. Oscillation Condition.

In an article by Vanier[4] the theory of the rubidium 87 maser had been given. In order to obtain a mathematical closed-form solution of the operation of the maser, the following assumptions were made in the analysis :

1) Reradiation was assumed to be completely quenched by the nitrogen buffer gas in the absorption cell.

2) The decay from the excited states took place randomly with equal probability to any of the ground states.

3) In the ground state, in the absence of light, relaxation taking place through collisions produced an equilibrium situation with all atoms equally distributed among the eight Zeeman sub-levels shown on figure 2.

4) The incident light consisted of the line $P \rightarrow S$, $F=2$ only. In other words, an ideal Rb 85 filter was assumed.

Furthermore, the hypothesis was made that the pumping rate was

homogeneous throughout the storage bulb in the cavity. Obviously, this assumption is not satisfied in practice but it was necessary in order to obtain a simple expression for the oscillation condition of the maser.

In more recent works we have removed this last assumption and have carried out a detailed calculation on the power output and oscillation condition of the maser on a digital computor. The detail of this theory is given in Appendix A, whose main steps are given here.

The pumping rate Γ given in number of photons per atoms per second is defined as

$$\Gamma(z,r) = \int_0^\infty I(\nu,z,r)\sigma(\nu)d\nu \quad , \tag{1}$$

where z is measured from the entrance of the bulb, r is the radial coordinate, in a cylindrical system, I is the intensity of incident light and σ is the cross section for absorption of a photon. The intensity decreases along z according to the law,

$$dI(\nu,z,r) = -I(\nu,z,r)\sigma(\nu)n(z,r)dz \quad ,$$

where n is the density of absorbing atoms at the coordinates (z,r) and is given by

$$n(z,r) = \frac{3\gamma_1 n_0}{5\Gamma + 8\gamma_1}\left[1 + \frac{16}{3}\frac{\Gamma(\Gamma+\gamma_1)\beta^2}{\gamma_1\left(\frac{\Gamma}{2}+\gamma_2\right)(5\Gamma^2 + 13\gamma_1\Gamma + 8\gamma_1^2) + 4\beta^2(2\Gamma^2 + 9\gamma_1\Gamma + 8\gamma_1^2)}\right] \tag{2}$$

where γ_1 and γ_2 are respectively the rate of decay of the diagonal and non diagonal elements of the density matrix; n_0 is the total number of atoms per unit volume; β is equal to $\frac{1}{2}(\mu_0 H_z/\hbar)$ where μ_0 is the Bohr magneton and H_z is the longitudinal component of the r.f. field in the cavity. The field is given by an expression such as $J_0(\sigma_2 r/R)\sin\pi z/\ell$ where σ_2 is the

second non zero root of $J_1(x)$, R is the radius of the cavity and ℓ its length. The variation of Γ as a function of the distance z is given on figure 3 for various parameters.

The power emitted by a small ring $2\pi r\,dr\,dz$ between the planes $z+dz$ and z, and between the cylinders r and $r+dr$ is given by

$$d^2P = \frac{h\nu n_0 2\pi r\,dr\,dz\,4K_1P\dfrac{J_0^2\left(\frac{\sigma_2}{R}r\right)}{J_0^2(\sigma_2)}\sin^2\frac{\pi z}{l}\,\Gamma(z,r)A(\Gamma)}{\gamma_1[\tfrac{1}{2}\Gamma(z,r)+\gamma_2]+8K_1P\dfrac{J_0^2\left(\frac{\sigma_2}{R}r\right)}{J_0^2(\sigma_2)}\sin^2\frac{\pi z}{l}\,[1-\Gamma(z,r)B(\Gamma)]} \qquad (3)$$

The total power emitted is :

$$P = \int_0^{\ell}\int_0^{R} d^2P \quad , \qquad (4)$$

which, for continuous oscillation, must be made self-consistent with the power lost in the cavity. Since the pumping rate $\Gamma(z,r)$ depends itself on the power of the maser through the density $n(z,r)$, it is obvious that one cannot obtain a solution in analytical form. However, we have solved the problem on an IBM 360 computor and have obtained the form of the power output versus the light intensity for various cavity quality factors. We have also determined the threshold conditions for oscillation as a function of γ_1 and $\eta Q_{c\ell}$ (detailed in Appendix A). Figures 4, 5, 6, 7, give the essential of these theoretical results. The results of these calculations can be compared with actual experimental results published by various authors. The order of magnitude of P_{max} is correct and the overlapping of the regions of oscillation for various γ_1 is in agreement with the experimental data. These points will be discussed further in the section treating of the experimental results.

2. Stability Considerations.

The stability of the masers has to be considered separately for short and long averaging times.

a) Short term stability.

The expression "short term" is rather loosely defined. In the present text we consider as short term, averaging times of the order of one second or less.

The short term stability of atomic oscillators has been considered in detail by several authors. The basic result is usually expressed in term of a variance of several measurements. Cutler et al[8] have shown that the maser fractional frequency stability is given by

$$\sigma(\langle\dot{\phi}\rangle_{t\tau}) = \left\{\frac{kT}{2P}\left[\frac{F\omega_1' Q_e}{\omega_0^2\tau^2 Q_{c\ell}} + \frac{1}{Q_\ell^2\tau}\right]\right\}^{1/2} \quad . \tag{5}$$

In this expression T is the temperature in Kelvin, k is Boltzman constant, P is the power output of the maser, F is the noise figure of the receiver, ω_0 is the resonance frequency, ω' is the filter cut off frequency, Q_e is the cavity external Q, $Q_{c\ell}$ is the loaded cavity Q, Q_ℓ is the atomic line Q and τ is the averaging time. In the expression above we assume a filter bandwidth large compared to $1/\tau$. The first term on the right of equation (5) is the so-called additive noise and the last term is the noise in the bandwidth of the atomic oscillator itself. The importance of the first term decreases as τ^{-1} while the size of the second term decreases as $\tau^{-1/2}$. Stability measurements as a function of the averaging time τ thus gives the possibility of answering the question as to which term is important. Another parameter used in specifying short term stability is the so-called Allan-

Variance[9]. In this case calculations show that an expression similar to equation (5) is obtained[10].

The expression above has been used extensively to compare atomic oscillators. It has been claimed that below $\tau = 1$ sec the rubidium maser would be characterized by the smallest σ or in other words the greatest stability.

It may be pointed out that it is mainly on this basis that the development of rubidium masers has taken place. As it will be shown in the section treating of the experimental results, this prediction was well founded.

b) Long term stability.

The long term stability of the maser is controlled by several factors of which the most important are :

- light shifts stability (spectrum stability),
- stability of the pressure (or density) of the rubidium vapor and of the buffer gases in the absorption cell,
- cavity pulling.

The two first effects are similar to those observed in passive rubidium standards and are expected to be of the same order of magnitude. It is a fact that in passive standards long term drifts of unknown origins are taking place. It is not known for sure yet if these drifts are mostly due to long term aging of the lamp, filter cell or absorption cell. Another program has been initiated in our laboratory on this subject and is briefly described in section VII. However, the most important effect expected to influence on the long term stability of the maser is the cavity pulling. The maser frequency offset due to a mistuning $\Delta\nu_c = \nu_c - \nu_0$ of the maser cavity, is given by :

$$\Delta\nu_m = \frac{Q_{\ell c}}{Q_\ell}\,\Delta\nu_c \quad . \tag{6}$$

In this expression $\Delta\nu_m$ is the maser frequency offset equal to $(\nu_m - \nu_0)$, where ν_m is the maser output frequency, $Q_{\ell c}$ is the loaded cavity quality factor, and Q_ℓ is the line Q of the maser atomic transition. ν_0 is the atomic resonance frequency including the shifts due to the presence of the buffer gas, the magnetic field and the light, and ν_c is the cavity resonance frequency. The expression above can be manipulated in the following way. If I is the intensity of the incident pumping radiation we may write :

$$\nu_0 = \nu_{00} + \alpha I \tag{7}$$

$$\Delta\nu_\ell = \Delta\nu_{\ell 0} + \beta I \tag{8}$$

where ν_{00} and $\Delta\nu_{\ell 0}$ are respectively the rubidium frequency and the width of the hyperfine line without the effect of the light. The terms α and β are factors which represent respectively the shift and broadening due to the light. The value given by equations (7) and (8) can be replaced in equation (6) and we obtain :

$$\nu_m \cong \nu_{00} + \alpha I + (\nu_c - \nu_{00})\,\frac{Q_c}{Q_{\ell 0}}\left(1 + \frac{\beta I}{\Delta\nu_{\ell 0}}\right) \quad . \tag{9}$$

The values of α and β are best determined experimentally. However, they are related to the pumping rate Γ defined earlier and to the line shape. In principle they can be calculated from basic theory. Appendix B gives expressions for α and β. Unfortunately, the actual spectrum of the lamp as seen by the absorption cell can be obtained only from experiments. Consequently, in order to explain the frequency biases observed, some knowledge of the lamp spectrum after filtering has to be obtained. Section IV describes the method we have used to obtain this data, through the use of a high resolution Fabry-Perot interferometer.

From equation (9) it can be shown that a particular setting of the cavity tuning can be found which will give a maser output frequency independent of light intensity. This setting is given by

$$\nu_0 = \nu_{00} - \frac{\alpha}{\beta} \frac{Q_{\ell 0}}{Q_c} \Delta\nu_{\ell 0} \quad . \tag{10}$$

This result is the direct consequence of the assumption that the light shift αI is a linear function of the intensity. Consequently, a given cavity setting can be found which will produce a maser output frequency independent of the light intensity. Experiments made to verify these predictions are described in section IV. Equation (9) dictates that, to obtain a frequency independent of the light intensity, the cavity must be mistuned by an amount equal to

$$\Delta\nu_c = - \frac{\alpha}{\beta} \frac{Q_{\ell 0}}{Q_c} \Delta\nu_{\ell 0} \quad . \tag{11}$$

The term α is the light shift factor and has to be known in order to evaluate the stability required from the lamp spectrum. It cannot be evaluated easily from the above expression, since the determination of $\Delta\nu_c$ requires an independent determination of the cavity tuning and of the light broadening. Methods of tuning may include the setting of the cavity resonant frequency for maximum power output or, better, the broadening of the resonance line through the excitation of transitions between the Zeeman levels. Theory shows that if all levels of the state $F = 2$ are equally populated, the excitation of such transitions will produce a pure broadening of the hyperfine line without frequency shifts. Effectively, in such a case equation (6) applies and for the purpose of tuning, Q_ℓ can be modulated by the introduction of Zeeman transitions.

From these expressions, it is clear that the cavity resonant frequency must be kept constant if long term stability is desired. In fact, for $Q_\ell \simeq 10^8$ and $Q_{\ell c} \simeq 35{,}000$ the cavity tuning must stay within approximately 20 Hz for a long term fractional stability of one part in 10^{12}. This is a rather stringent requirement, and it appears that servo techniques need to be developed to keep the cavity tuned to the frequency desired.

III. MASER ASSEMBLY

The two masers assembled in our laboratory are very similar and the description of only one is given here. The maser described is the one named NAS 1. A complete schematic diagram of the maser is shown on figure 8.

1. Cavity and Bulb.

The maser is of the "quartz cavity - quartz bulb" type. The storage bulb is made of pure clear fused silica and is built to rigid specifications. It fits to the wall of the cavity as close as possible. Calculations have shown that in order to have a cavity Q compatible with the operation of the maser in a continuous mode, the bulb must be thin with walls fitting as closely as possible inside the cavity cylinders[11]. The characteristics of the NAS I maser are given in Table 1.

Table 1 : NAS I - Rb 87 maser

Cavity	Quartz cylinder
Top	Transparent wrinkled foil
Bottom	Opaque
Bulb	Quartz (fused silica)
Q_u	34,700
$Q_{\ell c}$	variable
β	variable

The cavity quartz cylinder is silver-plated on the inside. The top, which is used for coarse tuning, is made of copper wrinkled foil and is transparent to the pumping light. The bottom which is also made of copper is not transparent. The arrangement provides a certain amount of compensation against temperature variations although no efforts have been made to design the system such as to provide optimum characteristics relative to long term frequency stability. Rough measurements, however, have shown that the cavity tuning was not too sensitive to temperature, and it was found that for the present task the results obtained were satisfactory.

The cavity itself is surrounded by a copper jacket on which is mounted the heater elements. This arrangement is necessary to avoid large gradients that would exist, if the heaters were mounted directly on the quartz cavity which has a poor thermal conductivity. Even with this arrangement it was necessary at high temperatures to add heater elements on the copper ends of the cavity to minimize the gradients.

The fine tuning of the cavity is accomplished through a small plunger at one of the end plates. The coupling is done through a coupling loop at the same end and is variable with a control external to the maser.

The storage bulb was filled on a high vacuum gas filling system. Rubidium was prepared directly in the bulb tip through a reaction of $RbC\ell$ with calcium metal chips. The buffer gas used is nitrogen at a pressure of approximately 11 torr.

In order to prevent condensation of rubidium on the walls of the storage cell, which would degrade the Q of the cavity through microwave losses, the bulb tip is maintained at a temperature a few degrees lower than the bulb itself.

2. Lamp and Filter.

The lamp consists of a large 7.5 cm mirror and of a 2.5 cm pyrex bulb. The bulb is filled with krypton at a pressure of a few torr and contains traces of rubidium 87. The bulb is placed in a region of the mirror which includes the focal point. It is surrounded by a radio frequency coil which forms the tank circuit of an oscillator operating at a frequency of approximately 80 MHz and delivering about 20 watts. With this power the lamp does not require external heating and the plasma losses are enough to maintain the temperature required for operation. The electronic circuit consists mainly of a 3E 29 vacuum tube and no particular efforts have been made to reduce its size, power consumption or other physical parameters. This type of lamp is found to operate well and is relatively stable. However, it is rather bulky and in future models it would be desirable to redesign it completely with the use of transistorized circuits.

The filter cell is of the standard type used in optical pumping experiments. It is made of pyrex and is approximately 7.5 cm in diameter and 3.7 cm long. It is filled with argon at a pressure of about 50 torr and contains traces of rubidium 87. The purpose of the argon buffer gas is to shift the spectrum of the rubidium 85 atoms towards the red. Through this effect the line $S_{1/2}$, $F=3 \leftrightarrow P$ of the rubidium 85 isotope coincides with the line $S_{1/2}$, $F=2 \leftrightarrow P$ emitted by the rubidium 87 lamp. This last line is absorbed and intensity pumping is obtained in the maser bulb.

The behaviour of the lamp and filter was analyzed on the high resolution Fabry-Perot interferometer. The results are given in section IV. It is sufficient, at this stage of the report, to say that the arrangement lamp-filter described here operated well and permitted the successful opera-

tion of the masers between the field independent levels in a continuous mode.

3. The Magnetic Field.

The magnetic field necessary to give to the system an axis of quantization which permits the operation in a field independent mode, is created by a large solenoid surrounded closely by a single magnetic shield made of moly permalloy. The solenoid is approximately 35 cm in diameter by 90 cm in length. The design of the shield and solenoid was borrowed directly from the hydrogen maser technology. This was done in order to save time. It provides an homogeneous magnetic field environment, but it is clear that the external physical appearance does not give justice to the actual size of the rubidium maser. The cavity which is the main part is only 12.5 cm in diameter and consequently could be surrounded by a smaller magnetic shield-solenoid arrangement.

The homogeneity produced by the arrangement is sufficient to obtain oscillation in a rather low field. In fact, continuous oscillation was observed without a decrease in amplitude at fieldsas low as 3×10^{-3} gauss. This is in contrast to the difficulty of operating hydrogen masers at low fields. This is due to the difference in principle of operation of the two devices.

In the hydrogen maser the atoms move freely in a bulb and see transverse inhomogeneities in the field, as a time varying magnetic field. If these inhomogeneities are large, the spectral density of this time varying phenomenon may be large enough to produce transitions between the Zeeman levels of the atoms. This produces a loss of coherence and may even quench the maser oscillation.

In the rubidium maser the atoms are effectively at rest, due to the presence of the buffer gas. Consequently, the inhomogeneity in the field causes mostly a broadening of the levels. Due to the fact that the relaxation created by spin exchange interactions is rather large, strong magnetic field inhomogeneities can be tolerated before any effects on the maser power output are observed.

It should be pointed out however that the single shield arrangement is not sufficient. The maser frequency is dependent on the position of the surrounding equipment. The effect of moving steel benches may produce shifts of the order of several parts in 10^{12}.

4. The Electronics.

The electronics associated with the maser has essentially two purposes: 1) maser control, 2) signal detection.

1) The maser electronics consists of a multi-point temperature control and of a magnetic field control.

The circuit used to control the temperature of the masers operates at a few kilohertz in a proportional mode. The energy is supplied to the heaters in the form of current pulses and the circuit controls the duty cycles of the pulses. Measurements have shown that with modest insulation, the gain of the system was sufficient to maintain a temperature stability better than 0.01°C during a day with external temperature variation of a few degrees.

The current necessary to control the magnetic fields is derived from a regulated power supply through voltage division in series resistance.

2) The maser signals are detected with the help of a sensitive super-

heterodyne receiver. Figure 9 is a schematic diagram of the system. It consists of a L.E.L. mixer preamplifier, a General Radio i.f. amplifier and a local oscillator. The local oscillator is made of a crystal oscillator at a frequency of 10.468 MHz multiplied by a factor of 650. The i.f. frequency is 30 MHz ; sometimes it is desirable to obtain a low frequency beat between the maser and the local oscillator ; this is done by a simple addition of a weak 30 MHz signal at the input of the i.f. amplifier. The frequency of the low frequency signal can then be varied by changing slightly the frequency of the local oscillator.

The masers do not normally operate immediately after the assembling of all the parts. There are too many parameters which control the threshold of oscillation, and adjustment of each of them needs to be done separately. This is done by stimulating the maser into transient oscillations with short r.f. pulses at the hyperfine frequency. It is then possible to adjust all the various parameters by looking at the signal output and to obtain continuous oscillation. The r.f. pulses at 6.834 GHz are generated from a system similar to the one used for the local oscillator, including a multiplication chain and a crystal oscillator. This system is also illustrated on figure 9.

IV. EXPERIMENTAL RESULTS

1. Power Output vs Light Intensity.

Experiments have been carried out in order to determine the light intensity for maximum power output at various cavity temperatures. The results of these experiments are shown on figure 10. Temperature is the parameter which is varied from one curve to another. The light intensity was varied either with a calibrated iris or neutral density filter. Both tech-

niques gave similar results.

The measurements were done through the receiver described earlier. This receiver was calibrated with the help of attenuators and a source whose output power was measured with a power bridge. The results obtained can be compared to the results of the calculations made earlier. No attempts have been made to adjust the parameters in order to obtain exact agreement between theory and experiment. However, it may be mentioned that the measured power output of the masers and the shape of the curves obtained is consistent with the results predicted by the theory.

It is difficult to obtain a precise value of the parameter η. If we suppose $\eta \simeq 0.7$ and $Q_{c\ell} \simeq 35{,}000$, we have $\eta Q_{c\ell} = 24{,}500$. From figure 4, this would give a maximum atomic power of about 125×10^{-11} W. With a coupling parameter of the order of 0.05 we would then expect a maser power output of about 6×10^{-11} W. This is in fair agreement with the data shown on figure 10. The maximum of power reported on this figure varies from 3 to 5.3×10^{-11} W. Furthermore, the form of the curves agrees qualitatively with those obtained from the theoretical calculations. One notes also at the lower threshold of oscillation an inflexion point which is visible on the theoretical and experimental curves.

These experiments are necessary for later work on measurements of the maser stability. In fact, the power output of the maser must be known in order to interpret correctly the measurements of the maser stability in the short term range.

2. Light Shifts.

Measurements of the displacement of the maser frequency by the light are somewhat tedious. As mentioned in the theoretical section, the

light has several effects, two of which are important for the present discussion. There is first a direct effect of frequency shift which is characterized by the parameter α. There is also an indirect effect which is related to the broadening of the resonance and which influences the maser frequency when the cavity is not tuned to the proper frequency. This last effect is characterized by the parameter β.

We have made experiments in order to determine the mutual influence of these two effects on the maser frequency. It is to be noted that they are not independent. Any experiments which consists in varying the light intensity will give results in which the two effects are present. Furthermore, the light spectrum consists of the two lines D_1 and D_2 which are not of the same intensity; their shapes depend also on the temperature of the filter cell and this complicates the interpretation of the results by the introduction of another parameter.

We have carried out the experiments in the following way.

1) First the lamp spectrum was analyzed on the Fabry-Perot interferometer, in order to determine the shape and the shift of the maximum intensity of the lines as a function of the filter temperature. This was done in the following manner: the lamp filter arrangement to be analyzed was placed directly in line with the Fabry-Perot interferometer. Another lamp, used as reference, was oriented at 90° to the axis of the Fabry-Perot interferometer. A reflecting blade was placed on the axis of the interferometer and in the path of the two lamps. This blade was made to rotate slowly with the help of an intermittent motion gear which permitted the passage from one lamp to the other, while the interferometer was scanned. The interferometer consisted of two mirrors 3.7 cm in diameter and polished to $\lambda/200$. These mirrors were

spaced by 15 mm. This provided a scanning range of 10 GHz per order. The mirrors and spacers were mounted in a vacuum envelope with end windows polished to about $\lambda/4$ and the scanning was done by varying the pressure inside the vacuum enclosure. The parallelism of the mirrors could be adjusted with the help of three screws accessible from outside the vacuum envelope. The central spot of the ring figure obtained was detected with a photomultiplier through a mask having a small opening of 0.25 mm in diameter. The spectrum was recorded on an XY recorder.

A typical recording is shown on figure 11. Figure 12 gives the frequency displacement of the pumping line as a function of the temperature of the filter cell.

2) In a second step we have investigated the effect of the light itself on the maser frequency. Various curves have been plotted of the maser frequency versus cavity tuning for several light intensities. A typical result is shown on figure 13. It is seen that a crossing point exists where the maser frequency output is independent of light intensity. This point does not appear where the cavity resonance frequency coincides with the atomic resonance frequency. The coincidence of cavity and resonance frequency can be verified either by maximum maser power output or by the method of line Q modulation to be described below.

The problem of deciding which cavity tuning should be chosen has to be solved on the basis of stability. If the light spectrum and intensity are not stable, it would be desirable to set the cavity resonance frequency at the point where the maser frequency is independent of light intensity. On the other hand, if the cavity resonance frequency is not stable, it is then desirable to tune the maser in such a way as to have coincidence between the

cavity and the atomic resonance frequency. The cavity resonance frequency could then be locked to the maser line through a servo-system. It appears that the last situation described is the one encountered in practice in our masers. This is probably due to an insufficient thermal control of the cavity.

Parameters α and β could be obtained from the data if I_{00} was known. For a typical light intensity used in our maser the light shift is of the order of 10 Hz while the contribution of the light to the broadening of the hyperfine line is approximately 100 Hz. More elaborate experiments are required in order to obtain actual values of α and β. These experiments necessitate for example the use of interference filters in order to separate the effect of the D_1 and D_2 lines.

3. Long Term Stability.

The long term stability of the rubidium maser is controlled at the present time by two main factors: 1) light intensity stability, 2) cavity stability.

1) The stability of the light influences the maser frequency stability through the light shift. As was seen earlier this effect can be cancelled by adjusting the cavity resonance frequency at such a setting that no change in maser output is observed for various light intensities.

2) The cavity stability influences the maser frequency through the pulling of the atomic resonance. The formula describing this effect has been given earlier and can be written in a simple form when the light intensity is considered constant. Thus considering only the effect of cavity pulling we may write [see equation (6)]:

$$\nu_m - \nu_0 = \frac{Q_c}{Q_\ell} (\nu_c - \nu_0) \qquad (12)$$

where standard notation has been used and where Q_ℓ is defined such as to include all sources of broadening of the atomic resonance. As mentioned earlier the parameters of our system are such that a cavity stability of approximately ± 20 Hz is required if a stability of ± 1 part in 10^{12} is desired. At present, a comparison between our two masers has shown that the stability in the medium term (~ 1 hour) is of the order of 1 part in 10^{11}. No major efforts have been made to improve this characteristics. Actually we are operating with only one oven wound very close to the cavity ; the temperature stability under these circumstances is not good. A double oven with good thermal insulation would be desirable and should improve easily the long term stability.

4. Tuning of the Masers.

In general, by the condition of tuning, we understand a situation in which the maser output frequency is identical to the atomic frequency ν_0 including shifts such as those produced by the second order doppler effect, buffer gas or wall collisions and by the applied magnetic field. In the hydrogen maser, the shift due to spin-exchange is cancelled exactly in the tuning procedure by a mistuning of the cavity. Although this has not been proved for the rubidium maser the same situation is expected to exist. However, spin exchange shifts are small and even negligible compared to other shifts that are present such as buffer gas shifts and light shifts. Consequently, a tuning procedure for rubidium masers in general should not be oriented toward the cancellation of spin exchange shifts.

There are two methods of tuning that could be exploited in this type of maser. Both are based on line Q modulation, but the parameter varied

in each case is different.

A. Light Intensity Variation. In a previous section we have described the effect of the shifts and broadening, due to the presence of the light. This was done in a phenomenological way but nevertheless, it was found that the experimental data was in qualitative agreement with the basic pulling equation obtained.

On figure 13, the straight lines obtained for various light intensities cross at a unique point. This point could in principle be used as a criterion which would render the maser frequency independent of light intensity. However, there is a disadvantage to this. In order to reach this point the cavity must be detuned by an amount such that the maser power output becomes rather low. In certain cases the tuning of the cavity is so far from the actual atomic frequency that the oscillation condition is not satisfied.

B. Magnetic Quenching. The effect of magnetic quenching has already been exploited in the hydrogen maser as a tuning method[12,13]. There are two ways in which the effect can be used :

- Field gradient : In this method a magnetic field gradient is applied to the maser. The effect on the maser is to broaden the energy levels. In the hydrogen maser the atoms are freely moving in a given volume and transitions are excited among the Zeeman levels. This introduces a loss of coherence in the transition $F=1$ $M_F=0$ and $F=0$ $M_F=0$ with a broadening of the corresponding line. In the rubidium maser however the atoms, for all purposes, are fixed at a given point in space by the buffer gas, and the magnetic field gradient will produce an inhomogeneous broadening of the resonance line.

Thus, in principle, the technique could be used in both cases to tune the masers. However, there is always an uncertainty in this procedure.

The frequency of the field independent transition depends on the magnetic field through the relation

$$\nu_{hf00} = \nu_0 + 574\ B^2 \qquad \text{(Rubidium 87)}$$

where B is the applied magnetic flux density in gauss. If a field gradient is applied, the average squared field seen by the atom may be raised by a slight amount. Consequently there exists an uncertainty as to the constancy of ν_{hf00} during the tuning procedure which requires a variation of the gradient.

- Zeeman transition broadening: Another method consists in introducing transitions between the Zeeman levels with a transverse oscillating magnetic field. This has the effect of destroying partly the coherence in the hyperfine transition by effectively removing atoms from the levels connected by this transition. Andresen[14] has shown that in the case where all the Zeeman sub-levels are equally populated, the effect of Zeeman transitions is a pure broadening of the levels without shifts of the maser line.

The method was used successfully in our rubidium maser and figure 14 shows a typical result. The ratio of Q_c/Q_ℓ (slope) is rather large and modulation of Q_ℓ through Zeeman transitions does not alter much this slope. In order to make evident the tuning possibility the data for the higher slopes (lowest Q_ℓ) was subtracted from the data for the smallest slope (largest Q_ℓ). It is these numbers that are plotted on figure 14. With the present masers, we evaluate that we can tune the maser with an accuracy of the order of 1 part in 10^{11}.

In principle this method could be used as the basis for a servo system in which the maser would continuously be kept tuned at the point where the frequency is independent of the intensity of the audio field applied in

resonance with the Zeeman transitions.

5. Short Term Stability.

As mentioned in the introduction the interest in the rubidium maser was raised by the promise of a stability in the short term region, superior to the stability obtained with all presently existing devices.

In order to verify this prediction, the two masers were built as similar as possible and measurements on their stability were made. The comparison system used is shown on figure 15. The beat frequency measured between the two masers was of the order of 600 Hz which has facilitated the measurement of the stability in the short term region. This difference in frequency was due to a difference in buffer gas pressure in the two masers. Statistics on the signal were done automatically on a computing counter HP-5360-A. The results for various experimental situations are shown on figure 16.

The stability of the masers was also measured in various other ways. One method consisted in measuring directly the time elapsed during 1000 periods of the beat signal. The measured time of the order of 1.6 sec was then recorded through a digital to analog converter. The recording gave an indication of the stability over an averaging time of 1.6 sec and in the same time gave indications of the relative stability of the masers in the medium and long term region.

Another method consisted in mixing the 600 Hz beat signal with a signal derived from a stable crystal oscillator through a synthesizer. The slow beat frequency obtained was measured on a counter and its characteristics were determined.

All methods gave consistent results and it is believed that the

stability recorded here are representative of our rubidium maser signals as detected with the receiver described in section III. Extensive work is presently under way in order to compare our experimental data to the predictions of equation (9). It may be mentioned here that the τ^{-1} law predicted is obeyed by our experimental results.

Figure 17 gives a comparison of the rubidium maser stability as compared to other oscillators. The rubidium maser has the best stability in the short term region.

V. FUTURE PROGRAM

It appears that, due to encouraging results obtained up to now with the rubidium masers, further development should be made. The main aspects which need to be developed are :

1) Reduction in size of the actual maser set up, specially the part concerned with the magnetic field including solenoid and magnetic shield. The present size of the shield is of the order of 35 cm by 90 cm. This could easily be reduced to about 20 cm by 30 cm.

2) The lamp driving electronics should be transistorized.

3) An electronic system should be designed such as to lock a crystal oscillator to the maser output.

4) The thermal control of the maser should be improved.

5) The method of tuning through the technique of broadening the maser line by Zeeman transitions should be made automatic.

VI. CONCLUSION

In this report we have given details on the construction of the "quartz bulb - quartz cavity" type rubidium maser. We have given the results obtained with two of these masers. These results were concerned with tuning characteristics, medium term stability and short term stability.

The stability of the masers in the short term region is superior to any of the oscillators presently existing. On this basis it is believed that future development of the masers to reduce their size and improve their medium term stability is well justified.

VII. OTHER RELATED PROJECTS

Several other research projects carried in our laboratories are related closely to the work described in this report. These include studies of relaxation of rubidium upon collisions with buffer gas atoms and surfaces, rubidium maser oscillation aided by external feedback, studies of long term stability of passive rubidium gas cells, and studies of a rubidium 87 maser made with a vacuum tight cavity.

The project of long term stability of rubidium gas cells is in direct connexion with our maser work since any solution to the long term instability problem of the passive rubidium gas cell standard could, in principle, be applied to the rubidium maser. The project consists in localizing the major causes of instability in the passive standard. The experimental arrangement is essentially a bridge set up in which two absorption cells are pumped simultaneously by the same lamp. The system has been described in earlier reports[17], and is practically completed. Measurements should begin soon, and results will be reported later.

The other project connected with the study of the stability of a maser made with a vacuum tight cavity is well under way. The stainless steel cavity itself is completed ; it needs to be assembled and filled with the proper buffer gas and rubidium 87. After completion its characteristics will be studied and compared to the presently existing masers.

VIII. NEW TECHNOLOGY

During the course of this program, a new method of tuning the masers was developed. This method of tuning consists in broadening the maser line by inducing transitions between the Zeeman levels.

Appendix A

(English version of "Théorie du Maser au Rubidium 87" by M. Tessier and J. Vanier, Can.J.Phys. 49, 2680, 1971)

In this appendix we want to calculate the threshold of oscillation and the power output of the maser. We compare the results of the calculations to published data.

CALCULATIONS

(a) Variation of the pumping rate Γ.

We define Γ as

$$\Gamma(z, r) = \int_0^\infty I(\nu, z, r)\, \sigma(\nu)\, d\nu \qquad A(1)$$

where ν is the frequency, $I(\nu,z,r)$ is the light spectral density at coordinates z,r and frequency ν. We use cylindrical coordinates as shown on figure A-1 :

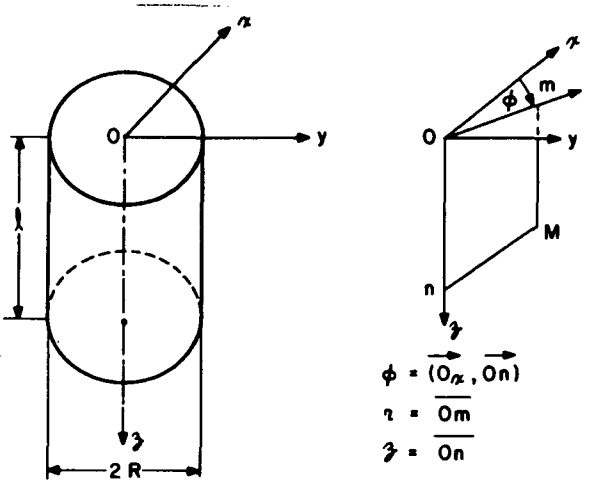

Fig. A-1 - Maser cavity and coordinate system.

We assume that the source spectral density is independent of r and we write :

$$I(\nu, 0, r) = I_0 = I_{00} \exp -\left[\frac{2(\nu - \nu_0)}{2\Delta\nu_D}\sqrt{\ln 2}\right]^2 \qquad A(2)$$

where ν_0 is the frequency of the peak of the line, $2\Delta\nu_D$ is its width and I_{00} is its maximum intensity. The absorption cross section can be written :

$$\sigma(\nu) = \sigma_0 \exp -\left[\frac{2(\nu - \nu_0)}{\Delta\nu_D}\sqrt{\ln 2}\right]^2 \qquad A(3)$$

This line is assumed to be twice as large as the emission line and centered on the same frequency. This hypothesis is based on experimental results obtained in this laboratory on a Fabry-Perot interferometer[15]. We assume that the light decreases along the axis of the storage bulb according to the differential equation :

$$d I(\nu, z, r) = - I(\nu, z, r)\ \sigma(\nu)\, n(z, r)\, dz \qquad A(4)$$

which says that the decrease in intensity between the planes z and $z + dz$ is proportional to the intensity at the plane z, to the absorption cross section, to the penetration dz and to the number of absorbing atoms $n(z,r)$ per unit volume. In this case we can show that[4,16] :

$$n(z, r) = \frac{3\gamma_1 n_0}{5\Gamma + 8\gamma_1}\left[1 + \frac{16}{3}\frac{\Gamma(\Gamma + \gamma_1)\beta^2}{\gamma_1\left(\frac{\Gamma}{2} + \gamma_2\right)(5\Gamma^2 + 13\gamma_1\Gamma + 8\gamma_1^2) + 4\beta^2(2\Gamma^2 + 9\gamma_1\Gamma + 8\gamma_1^2)}\right] \qquad A(5)$$

where γ_1 and γ_2 are respectively the decay rates of the diagonal and non-diagonal elements of the density matrix, n_0 is the density of atoms and β represents the expression $\frac{i}{2}(\mu_0 H_z/\hbar)$ in which μ_0 is the Bohr magneton, H_z is the longitudinal component of the r.f. field. The variation of H_z in the cavity (TE 021) has the form $J_0(\sigma_2 \nu/R)\sin(\pi z/\ell)$ where σ_2 is the second root of $J_1(x)$, R is the radius of the cavity and ℓ its length. It is useful to write β^2 in the following way :

$$\beta^2 = K\langle\beta^2\rangle J_0^2\left(\frac{\sigma_2}{R} r\right) \sin^2 \frac{\pi z}{l} \qquad A(6)$$

Here $\langle \beta^2 \rangle$ is the average value of β^2 over the cavity. The constant K is equal to $\left(2/J_0^2(\sigma_2)\right)$. We finally obtain :

$$\beta^2 = \frac{2}{J_0^2(\sigma_2)} \langle \beta^2 \rangle J_0^2\left(\frac{\sigma_2}{R} r\right) \sin^2 \frac{\pi z}{l} \qquad A(7)$$

The parameter $\langle \beta^2 \rangle$ is connected to the power delivered by the rubidium vapor or the power lost in the cavity walls and coupling loop by the relation

$$4\langle \beta^2 \rangle = \frac{8\pi Q_l \eta \mu_0^2}{\omega V_c \hbar^2} P_{diss} \qquad A(8)$$

where Q_ℓ is the loaded quality factor of the cavity and η is the filling factor defined by

$$\eta = \frac{\int_{V_c} H_z^2 \, dV}{\int_{V_c} H_{rf}^2 \, dV}$$

In these last expressions V_c is the volume of the cavity and ω is the angular frequency of the maser oscillations. To simplify we write equation A(8) as

$$\langle \beta^2 \rangle = K_1 P \qquad A(9)$$

where

$$K_1 = \frac{8\pi Q_l \eta \mu_0^2}{4\omega V_c \hbar^2} \qquad A(10)$$

With these definitions we can write equation A(4) as

$$\frac{dI(\nu, z, r)}{I(\nu, z, r)} = -\sigma(\nu) n(z, r) \, dz \qquad A(11)$$

We integrate over z and we obtain

$$\ln \frac{I(\nu, z, r)}{I_0} = -\int_0^z \sigma(\nu) n(z, r) \, dz \qquad A(12)$$

from which

$$I(\nu, z, r) = I_0 \exp -\int_0^z \sigma(\nu) n(z, r) \, dz \qquad A(13)$$

We replace in equation A(1) and we obtain :

$$\Gamma(z, r) = \int_0^\infty I_0\sigma(\nu)\left[\exp -\sigma(\nu)\int_0^z n(z, r)\,dz\right]d\nu \qquad A(14)$$

It can be shown that $\Gamma(z,r)$ can be written as[16]

$$\Gamma(z, r) = \Gamma_0\left(1 + \sum_{n=1}^{\infty} \upsilon_n\right) \qquad A(15)$$

where

$$\Gamma_0 = \Gamma(0, r) = \frac{I_{00}\sigma_0\Delta\nu_D\sqrt{\pi}}{2\sqrt{1.25\ln 2}} \qquad A(16)$$

and

$$\upsilon_n = \frac{(-1)^n}{n!\sqrt{\dfrac{n + 1.25}{1.25}}}\left[\int_0^z \sigma_0 n(z, r)\,dz\right]^n \qquad A(17)$$

The density $n(z,r)$ is a function of Γ and β^2, since β^2 is a function of P through equation A(8).

(b) Self consistent solution.

The power delivered by the element of volume $2\pi r\,dr\,dz$ *between* planes $z+dz$ and z and between the cylinders r and $r+dr$ is given by

$$d^2P = \frac{h\nu n_0 2\pi r\,dr\,dz\,4K_1P\dfrac{J_0^2\left(\dfrac{\sigma_2}{R}r\right)}{J_0^2(\sigma_2)}\sin^2\dfrac{\pi z}{l}\,\Gamma(z, r)A(\Gamma)}{\gamma_1[\tfrac{1}{2}\Gamma(z, r) + \gamma_2] + 8K_1P\dfrac{J_0^2\left(\dfrac{\sigma_2}{R}r\right)}{J_0^2(\sigma_2)}\sin^2\dfrac{\pi z}{l}\,[1 - \Gamma(z, r)B(\Gamma)]} \qquad A(18)$$

This equation is derived in a similar way as formula (18) of reference (4). Parameters A and B are

$$A(\Gamma) = \frac{\gamma_1(\Gamma + \gamma_1)}{5\Gamma^2 + 13\gamma_1\Gamma + 8\gamma_1^2} \qquad A(19)$$

$$B(\Gamma) = \frac{3\Gamma + 4\gamma_1}{5\Gamma^2 + 13\gamma_1\Gamma + 8\gamma_1^2} \qquad A(20)$$

The self consistent solution is obtained by integrating over the whole cavity volume

$$P = \int_0^l \int_0^R d^2P$$

P must then satisfy the following relation :

$$1 = 8\pi h\nu K_1 n_0 \times \int_0^l \int_0^R \frac{J_0^2\left(\frac{\sigma_2}{R} r\right) \sin^2 \frac{\pi z}{l} \Gamma(z, r) A(\Gamma) r \, dr \, dz}{\gamma_1 J_0^2(\sigma_2)[\tfrac{1}{2}\Gamma(z, r) + \gamma_2] + 8K_1 P J_0^2\left(\frac{\sigma_2}{R} r\right) \sin^2 \frac{\pi z}{l} [1 - \Gamma(z, r) B(\Gamma)]} \qquad A(21)$$

To solve this equation, we must know $\Gamma(z,r)$. However $\Gamma(z,r)$ depends on P through $n(z,r)$. We thus proceed as follows : we set Γ_0 and we start with $P = 0$. We determine $\Gamma(z,r)$ from equation A(15). To do this we assume a given $\Gamma(z,r)$ and to calculate $\Gamma(z+dz,r)$ we evaluate the second member of equation A(13) in assuming that $\Gamma(z+dz,r) = \Gamma(z,r)$. Proceeding this way several times we obtain $\Gamma(z+dz,r)$ with the desired accuracy. Since we know $\Gamma(0,r) = \Gamma_0$ we can then calculate $\Gamma(z,r)$ for all z. We then have to solve A(21) which gives a value of P. We then calculate again $\Gamma(z,r)$ using this new value of P and repeat the procedure. In practice, we obtain consistent results after 3 or 4 loops ; we have compared this method to analytical solutions that we can obtain in certain special cases and both agreed to about 1 part in 10^4.

In our calculations we have assumed the following numerical values :

$$\omega = 2\pi \times 6.8 \times 10^9 \text{ rad/s}, \qquad \ell = 8 \text{ cm}, \qquad R = 5 \text{ cm} .$$

Furthermore we do not differentiate between D_1 and D_2 lines emitted by the lamps and we set $\sigma_0 = 2 \times 10^{-11} \text{ cm}^2$. Finally we assume the following relations

$$n_0 = \frac{\gamma_1 - 10}{6.4} 10^{10} \text{ atomes/cm}^3$$

$$\gamma_2 = 63 + \frac{5}{8} (\gamma_1 + 10)$$

In each particular case, we set given values for γ_1, ηQ_ℓ and Γ_0. The numerical calculations have been made on a computor (APL 360).

(c) Results of the calculations.

(1) The pumping rate Γ.

We have obtained several curves of Γ as a function of z and a typical set of these curves is shown on figure 3.

We consider first the case where $P=0$. This is the case of oscillation threshold. Equations A(15) and A(21) are then independent of r. It is found that $\Gamma(z)$ decreases rapidly when the light beam penetrates inside the cavity. The hypothesis normally made that $\Gamma(z)$ is constant in the cavity is thus not realistic. For most cases we see that $\Gamma(z)$ at the bottom of the cavity is of the order of 1% of Γ_0 or less.

When $P \neq 0$, the pumping rate depends on r through the product $K_1 P J_0^2(\sigma_2 r/R)\sin^2(\pi z/\ell)$. To obtain $\Gamma(z,r)$, we assume given values for Γ_0 and P, and fix r. It is then found that for a given r, the decrease in Γ with z increases with increasing P, producing a transverse modulation of the pumping rate. The decrease of Γ is maximum on the cavity axis.

If we calculate $\Gamma(z)$ with the help of formula (57) of reference (4), which assumes rectangular shapes for light emission and absorption we obtain a faster decrease in $\Gamma(z)$ with z.

(2) The power delivered by the vapor.

Figure 4 gives the variation of the power output for two experimental situations. Figure 5 gives the variation of the maximum of power as a function of γ_1 assuming in each case sufficient light intensity to reach this maximum. The oscillation threshold as a function of γ_1 and ηQ_ℓ are also

given on figures 6 and 7 respectively. The results are qualitatively in agreement with those published earlier[4], but the absolute values of the maximum power output are smaller. It is found here that the power output is extremely sensitive to the value of ηQ_ℓ. For example if $\eta Q_\ell = 13{,}000$, $P_{max} = 0$; but if $\eta Q_\ell = 16{,}500$, $P_{max} = 41 \times 10^{-11}$ W while if $\eta Q_\ell = 25{,}000$, $P_{max} = 146 \times 10^{-11}$ W, γ_1 being equal to 140 s^{-1}. However, P_{max} tends to a limit when ηQ_ℓ becomes large. In the examples above, P_{max} is a strong function of ηQ_ℓ, because we are close to the threshold of oscillation. These results are interesting for the case where a quartz bulb is used in which case ηQ_ℓ is reduced by the presence of microwave losses.

The curve of $P_{max} = g(\gamma_1)$ is approximately a parabola which shows P_{max} is nearly proportional to γ_1^2 or n_0^2.

The region of Γ_0 over which maser oscillations are possible increases with γ_1 and ηQ_ℓ.

Appendix B

The starting point of the calculations on the effect of the light is taken from previous work by Barrat et al[18] and by Vanier[19]. From these results we obtain after averaging over the Doppler distribution, the following expression for the light shift parameter

$$\alpha = \frac{\sigma_0}{\pi} \int_{-\infty}^{\infty} \int_{-\infty}^{\infty} \frac{I(\nu)(\nu - \nu_a)}{(\nu - \nu_a)^2 + \left(\frac{\Delta\nu_a}{2}\right)^2} e^{-\frac{4(\nu_a - \nu_0)^2}{(\Delta\nu_D)^2} \ln 2} \, d\nu d\nu_a \quad ,$$

where ν_a is the line center frequency of a given class of atoms, ν_0 is the line center frequency of the doppler broadened line, $\Delta\nu_a$ is the natural line width, $I(\nu)$ is the light source spectral density and σ_0 is the absorption cross section.

For the light broadening parameter a similar expression can be derived:

$$\beta = \frac{\sigma_0}{\pi} \int_{-\infty}^{\infty} I(\nu) \, e^{-\frac{4(\nu - \nu_a)^2}{(\Delta\nu_D)^2} \ln 2} \, d\nu \quad .$$

In the case of the rubidium maser where $I(\nu)$ is a function of the coordinates in the storage bulb these integrals can be evaluated only numerically. These calculations have been done for the D_1 line. The results obtained indicate that although there is a very strong inhomogeneity in the pumping rates throughout the maser bulb (see figure 3), the maser light shift is still almost linear with light intensity. Furthermore, even in those conditions we find that the line is very nearly symmetrical.

References

1. P. Davidovits, Appl. Phys. Letters 5, 15, 1964.
2. P. Davidovits and W.A. stern, Appl. Phys. Letters 6, 20, 1965.
3. P. Davidovits and R. Novick, Proc. IEEE 54, 155, 1966.
4. Jacques Vanier, Phys. Rev. 168, 129, 1968.
5. R.F.C. Vessot, Quantum Electronics, proceedings of the third International Congress 409, 1964.
6. K. Shimoda, T.C. Wang and C.H. Townes, Phys. Rev. 102, 1308, 1956.
7. E.I. Alekseyev and Ye.N. Bazarov, Radio Engineering and Electronic Physics 15, 5, 1970.
8. L.S. Cutler and C.L. Searle, Proc. IEEE 54, 136, 1966.
9. D.W. Allan, Proc. IEEE 54, 221, 1966.
10. M. Têtu, G. Busca, J. Vanier (unpublished).
11. M. Tessier, J. Vanier, Can. J. Phys. 49, 1482, 1971.
12. J. Vanier and R.F.C. Vessot, IEEE J. of Quantum Electronics, QE 2, 391, 1966.
13. Jacques Vanier, Patent N° 3,435,369, Tuning of Atomic Masers by Magnetic Quenching using Transverse Magnetic Fields.
14. Harro G. Andresen, Z. Physik, 223, 71, 1969.
15. G. Missout, R. Vaillancourt, M. Têtu et J. Vanier, Rev. Phys. Appl. 6, 307, 1971.
16. M. Tessier et J. Vanier, Can. J. Phys. 49, 2680, 1971.
17. Third semi-annual status report to NASA on "Rubidium Gas Cell Studies", April 1, 1971 to September 30, 1971, N.G.R. 52-133-001.
18. J.P. Barrat and C. Cohen Tannoudji, J. Phys. Radium 22, 329 and 443, 1961.
19. Jacques Vanier, Can. J. Phys. 47, 1461, 1969.

Figure captions

Figure 1 Schematic diagram of the rubidium 87 maser.

Figure 2 Lower energy levels diagram of the rubidium 87 atom.

Figure 3 Theoretical variation of the pumping rate Γ as a function of the distance z in the absorption cell (Formula 57 refers to the article by Vanier[4]).

Figure 4 Theoretical atomic power as a function of the pumping rate Γ_0 at the entrance of the bulb.

Figure 5 Theoretical variation of the maximum power $P = f(\Gamma_0)$ as a function of γ_1.

Figure 6 Theoretical oscillation threshold as a function of γ_1 (ηQ_ℓ constant).

Figure 7 Theoretical oscillation threshold as a function of ηQ_ℓ (γ_1 constant).

Figure 8 NAS 1 Rb 87 maser assembly.

Figure 9 Superheterodyne receiver.

Figure 10 NAS 1 Rubidium maser power output as a function of light intensity.

Figure 11 Typical rubidium spectrum observed on the Fabry-Perot interferometer. The trace is alternated between the filtered lamp and a reference lamp by a rotating chopper. Figure 4a is for a lamp without filter, while 4b is for a hot filter. In figure 4a the lines coincide while in figure 4b one line is absorbed by the isotopic filter and the other is shifted.

Figure 12 Frequency displacement of the pumping line as a function of temperature of the filter cell.

Figure 13 Cavity tuning and light shift. The parameter varied from one curve to another is the light intensity.

Figure 14 Tuning of the rubidium 87 maser through the method of line Q broadening by Zeeman transitions in the field dependent levels.

Figure 15 Experimental set-up used to measure the rubidium masers frequency stability.

Figure 16 Rubidium maser stability in the short term region as a function of averaging time. The parameter varied from one curve to another is the power output of both masers.

Figure 17 Comparison of rubidium maser frequency stability to other existing oscillators.

Figure 18 Photograph of the two NASA rubidium 87 masers.

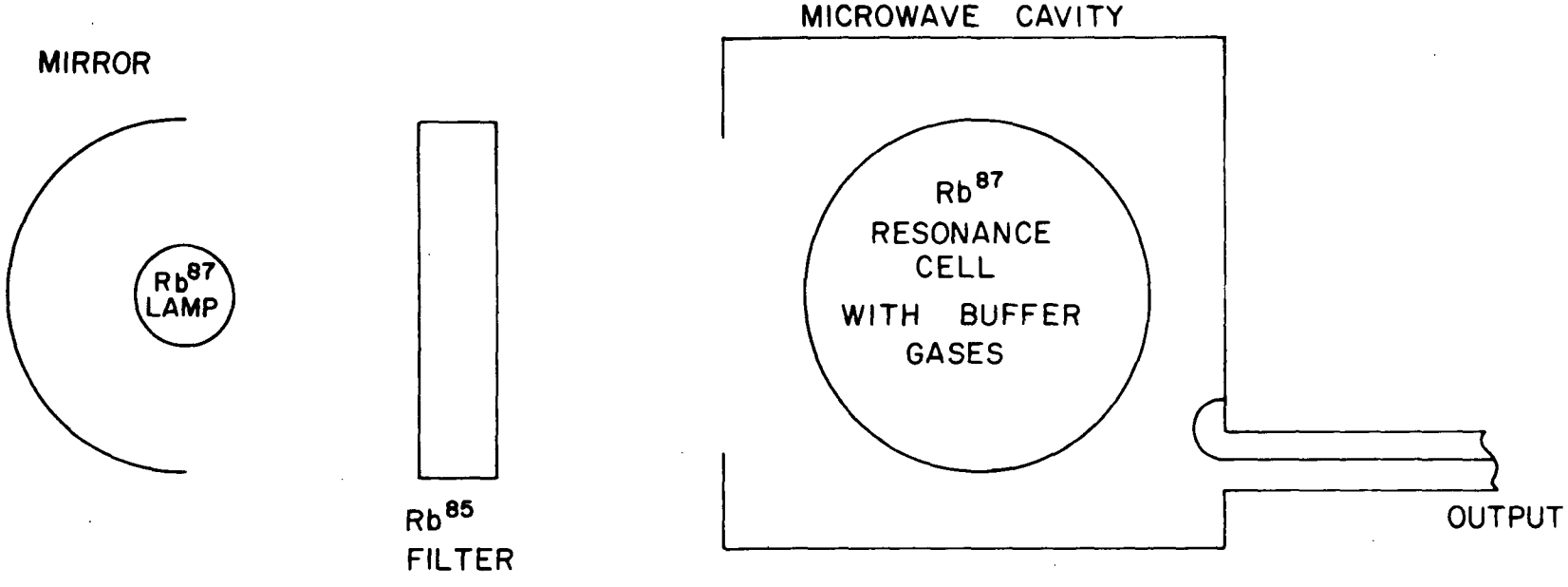
MIRROR
Rb87 LAMP
Rb85 FILTER
MICROWAVE CAVITY
Rb87 RESONANCE CELL WITH BUFFER GASES
OUTPUT

Figure 1

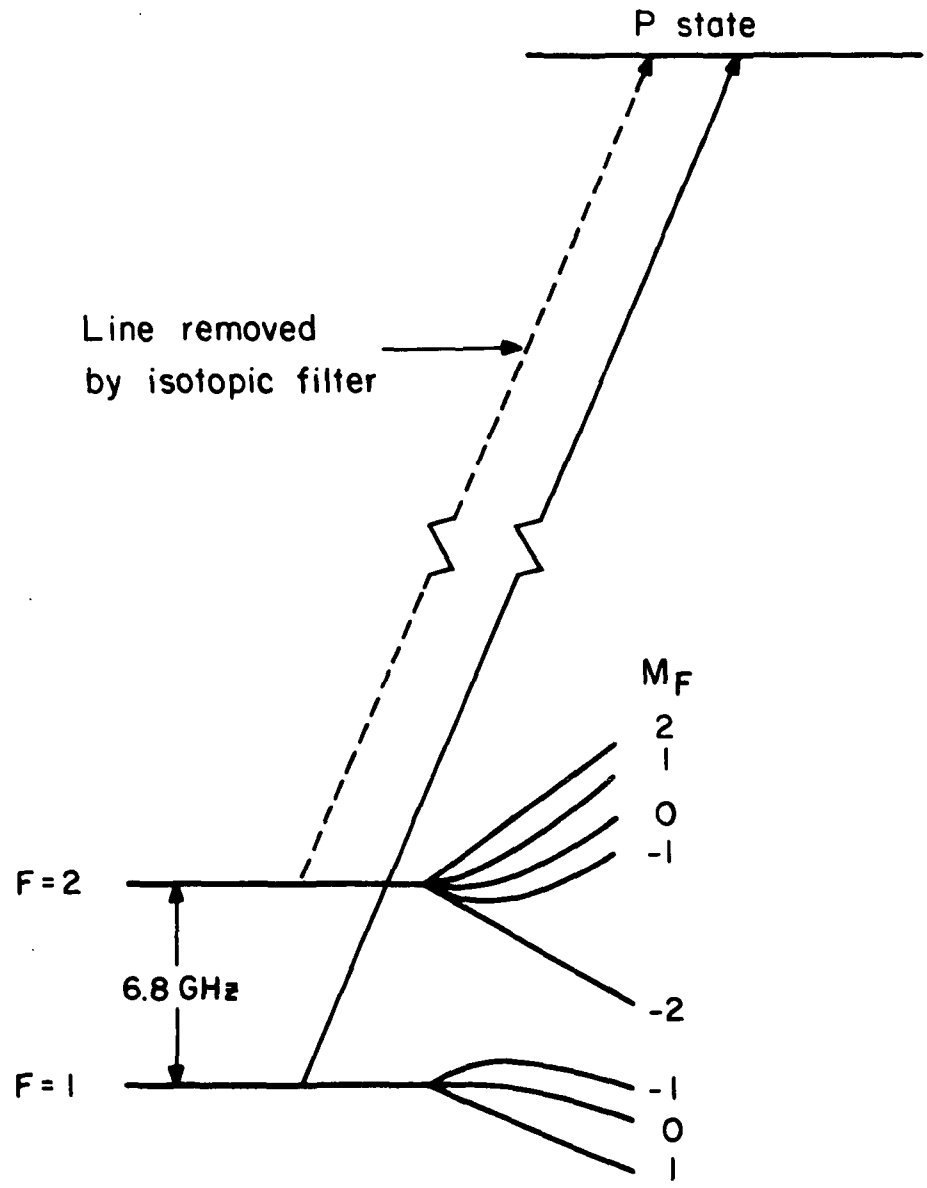
P state
Line removed
by isotopic filter
M_F
2
1
0
-1
-2
F = 2
6.8 GHz
F = 1
-1
0
1

Figure 2

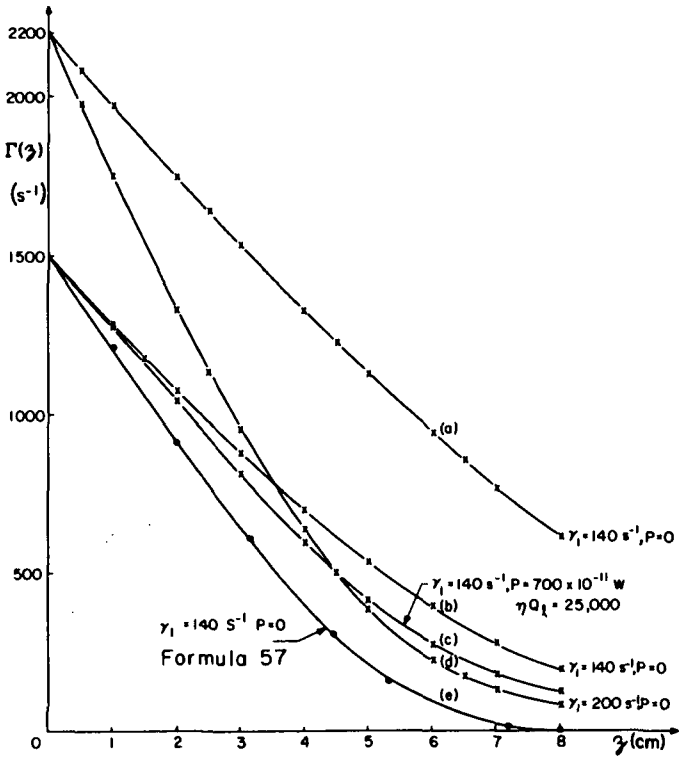

Figure 3

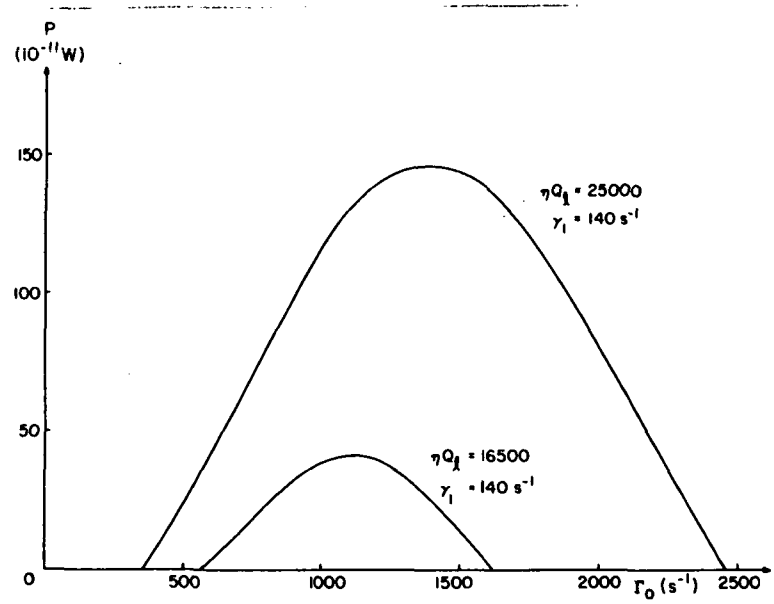

Figure 4

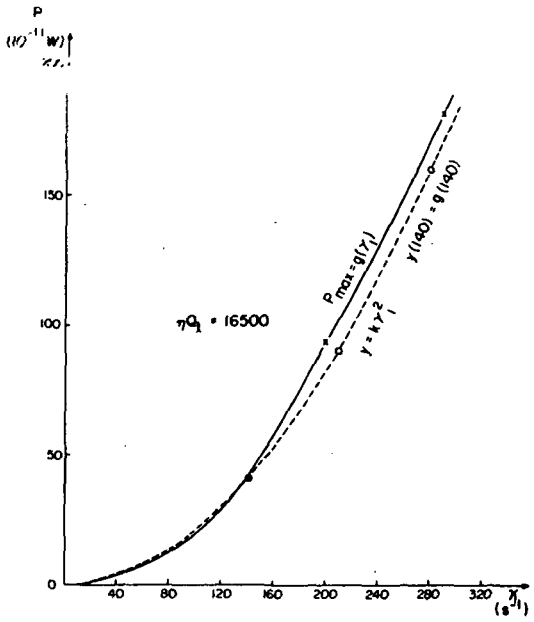

Figure 5

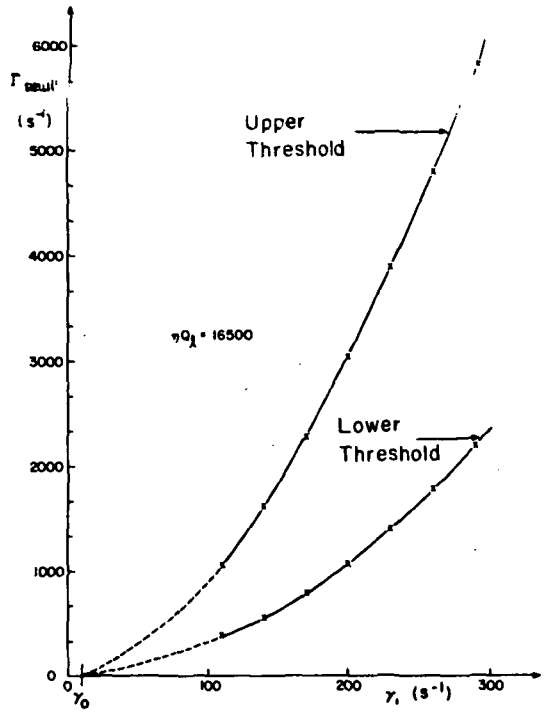

Figure 6

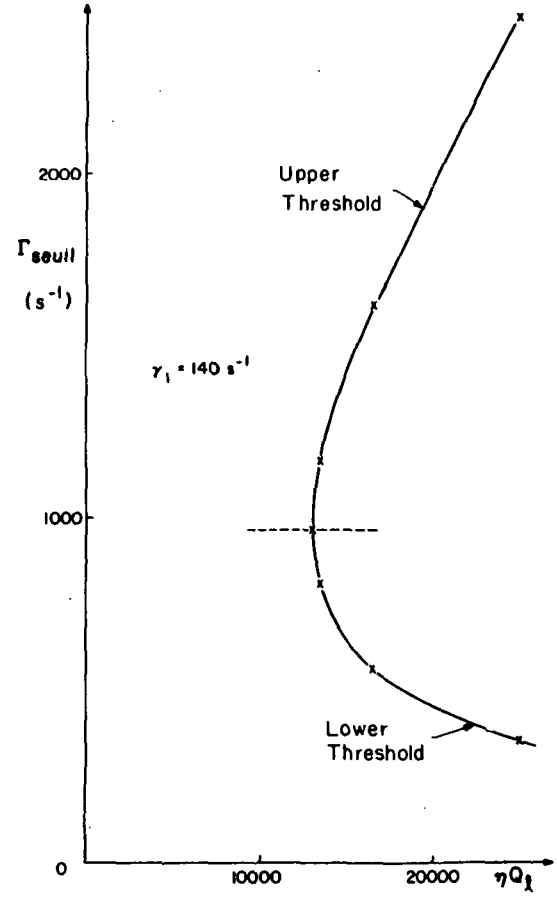

Figure 7

Rb 87 MASER SCHEMATIC DIAGRAM

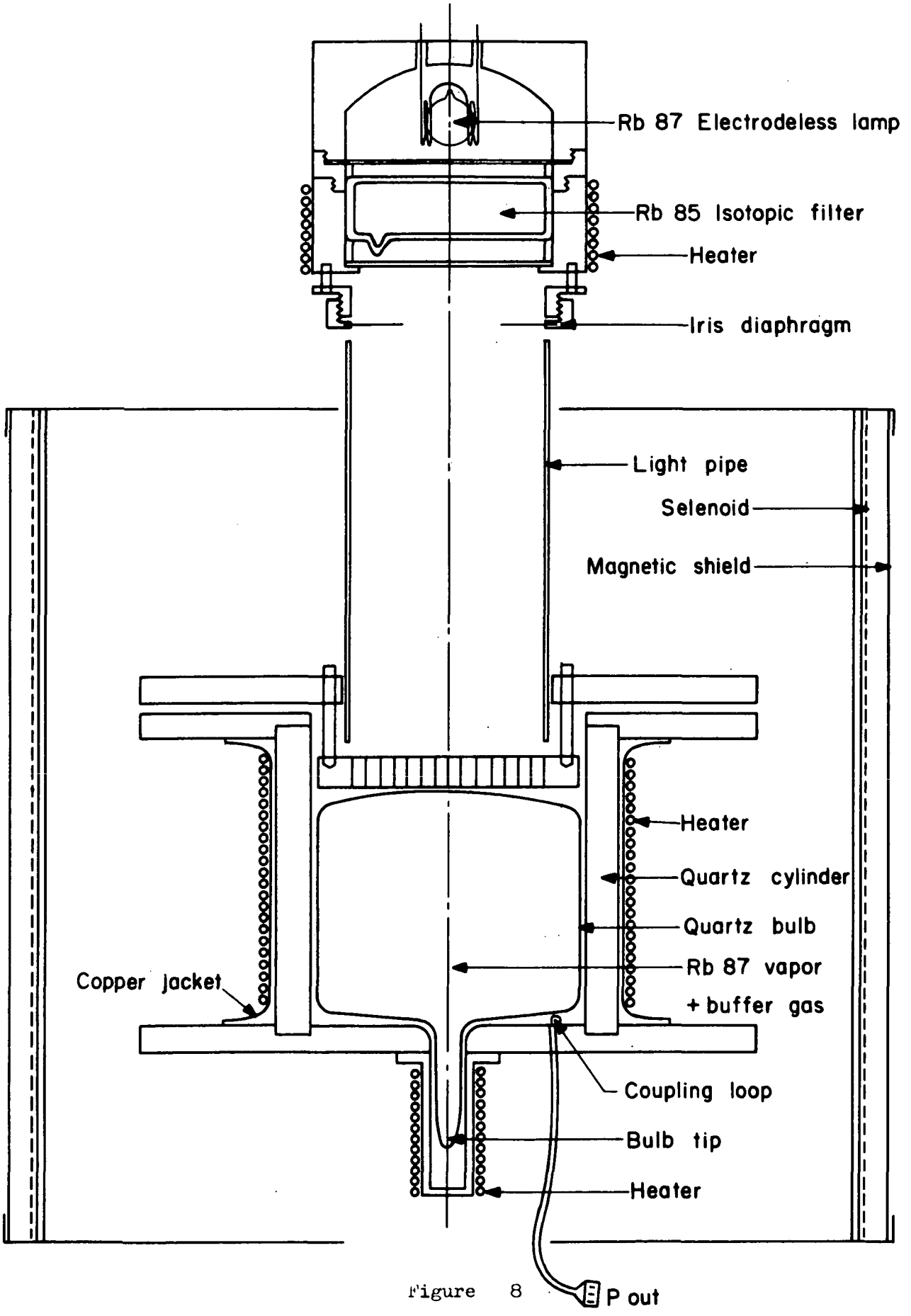

Figure 8

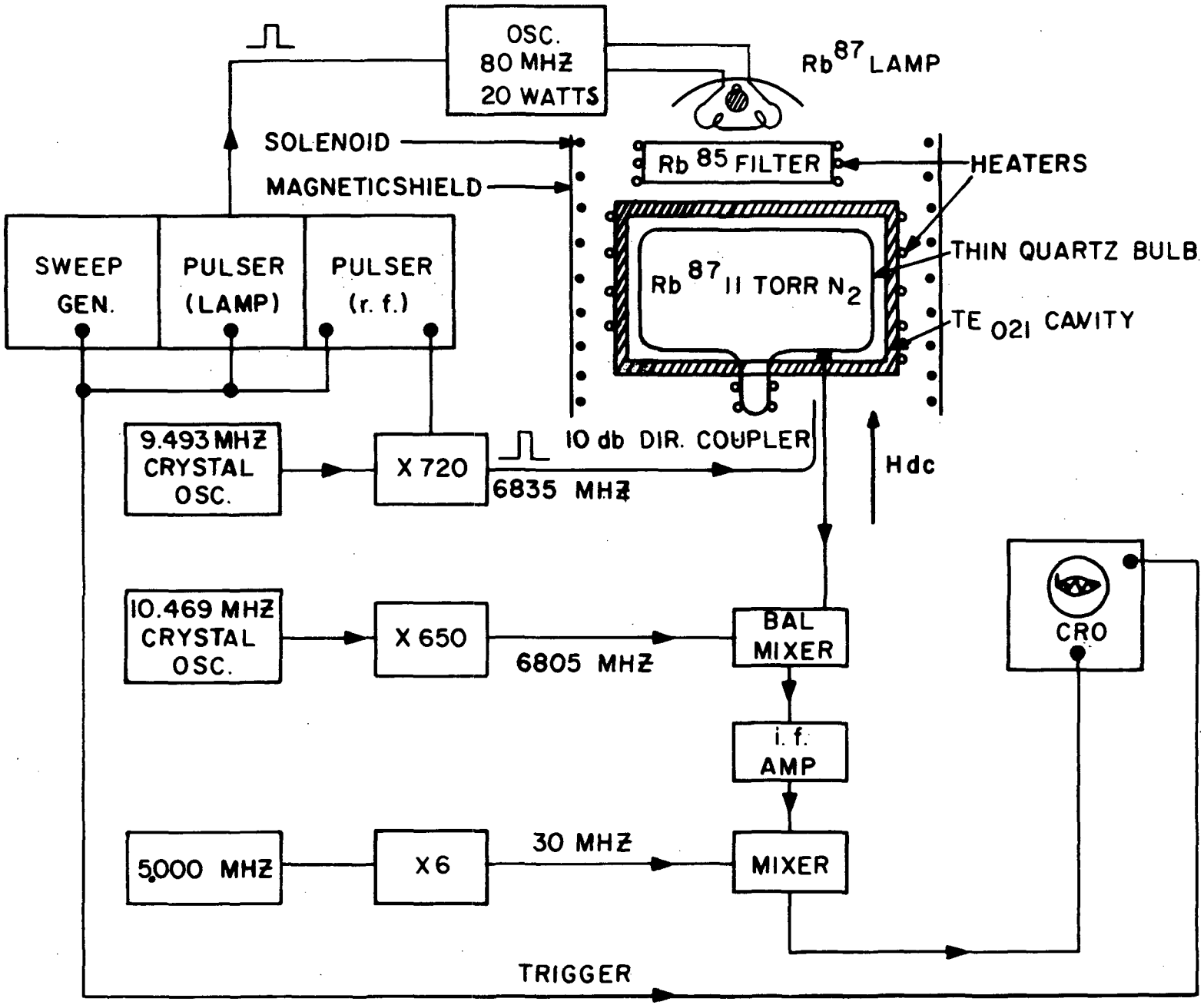
OSC.
80 MHZ
20 WATTS
Rb 87 LAMP
SOLENOID
MAGNETICSHIELD
Rb 85 FILTER
HEATERS
THIN QUARTZ BULB
Rb 87 11 TORR N2
TE 021 CAVITY
SWEEP GEN.
PULSER (LAMP)
PULSER (r. f.)
9.493 MHZ CRYSTAL OSC.
X 720
10 db DIR. COUPLER
6835 MHZ
Hdc
10.469 MHZ CRYSTAL OSC.
X 650
6805 MHZ
BAL MIXER
CRO
i. f. AMP
5000 MHZ
X6
30 MHZ
MIXER
TRIGGER

Figure 9

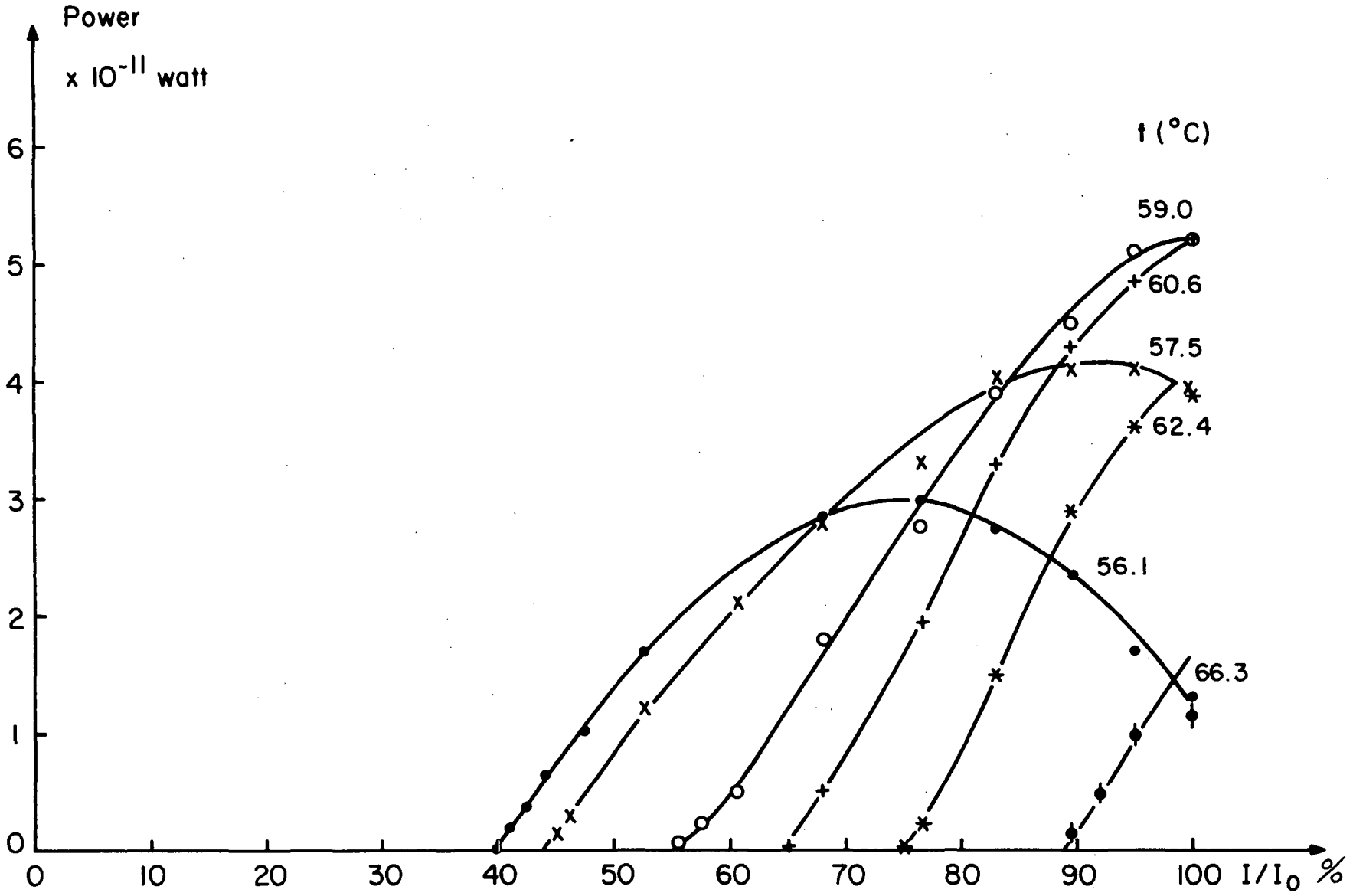
Power
x 10^-11 watt
t (°C)
59.0
60.6
57.5
62.4
56.1
66.3
0
1
2
3
4
5
6
0
10
20
30
40
50
60
70
80
90
100
I/I0 %

Figure 10

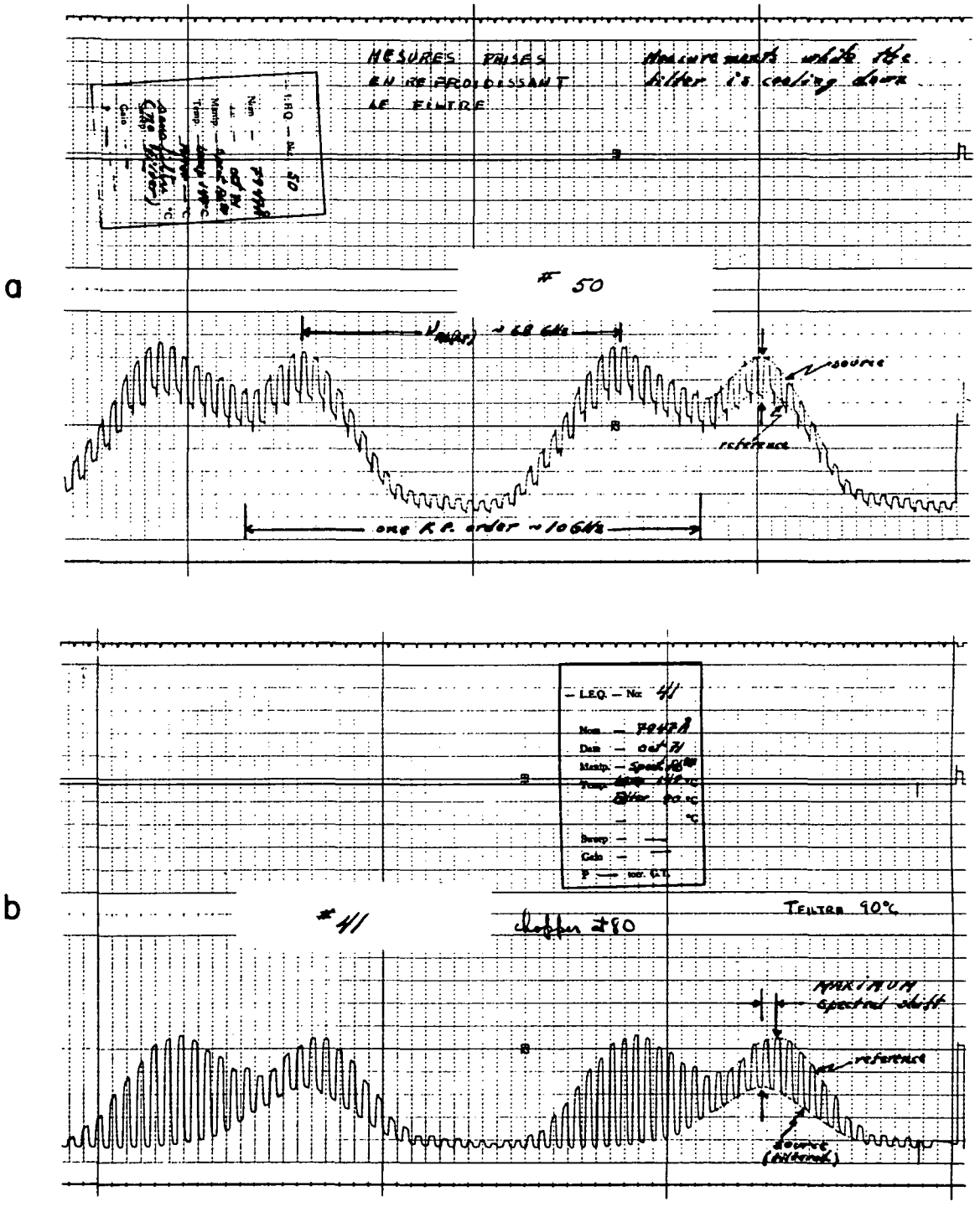
MESURES PAUSES
EN NE PROCESSANT
AE FILTRE
Measurements while the
filter is cooling down
a
50
source
reference
one R.P. order ~10Hz
b
41
Doppler ±80
TEILTER 90°C
MAXIMUM
Spectral shift
reference
source
(different)

Figure 11

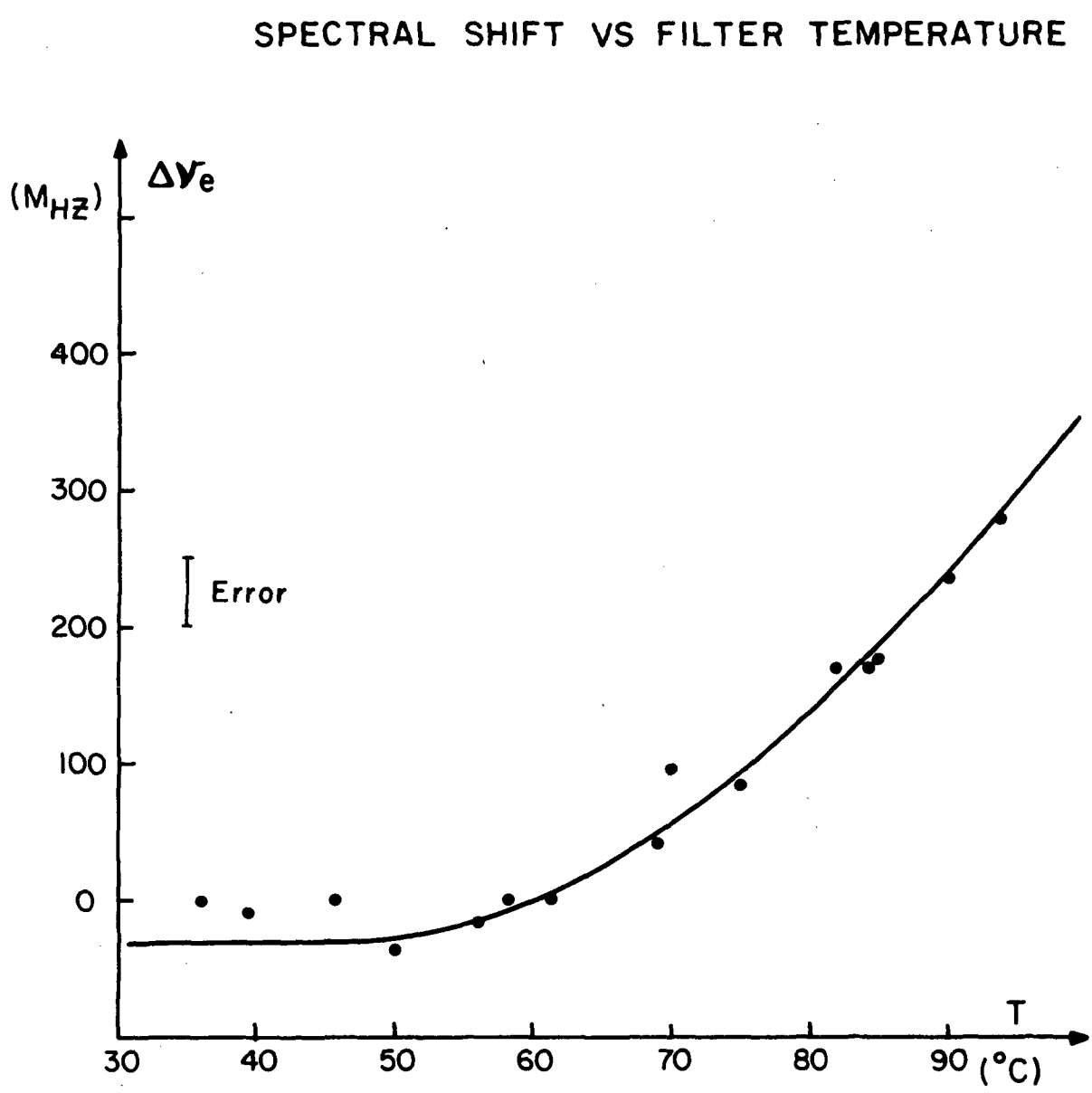
SPECTRAL SHIFT VS FILTER TEMPERATURE
(MHz)
ΔVe
400
300
200
100
0
Error
30
40
50
60
70
80
90
T
(°C)

Figure 12

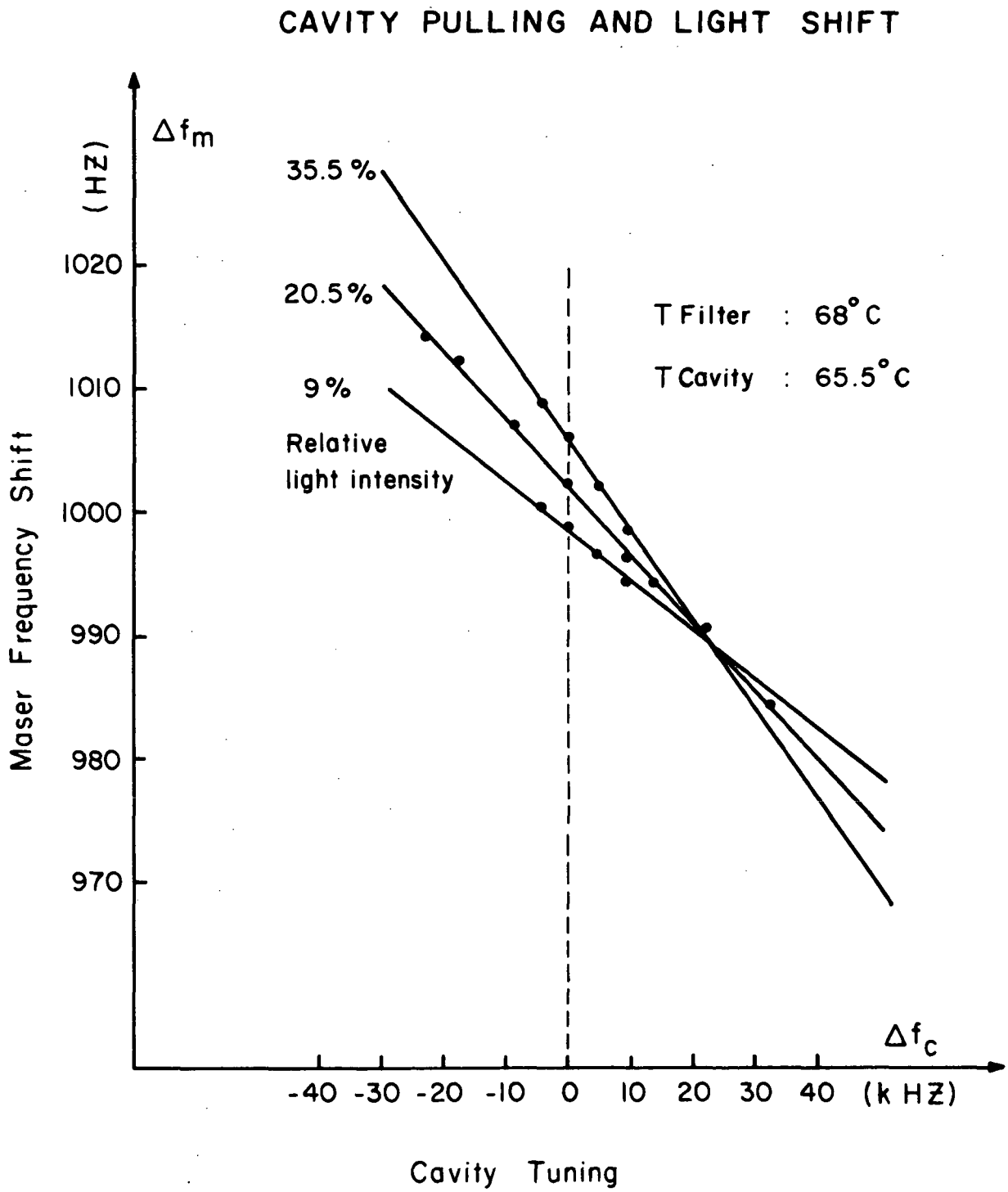
CAVITY PULLING AND LIGHT SHIFT
Δfm
(HZ)
1020
1010
1000
990
980
970
Maser Frequency Shift
35.5 %
20.5 %
9 %
Relative
light intensity
T Filter : 68°C
T Cavity : 65.5°C
Δfc
-40 -30 -20 -10 0 10 20 30 40 (k HZ)
Cavity Tuning

Figure 13

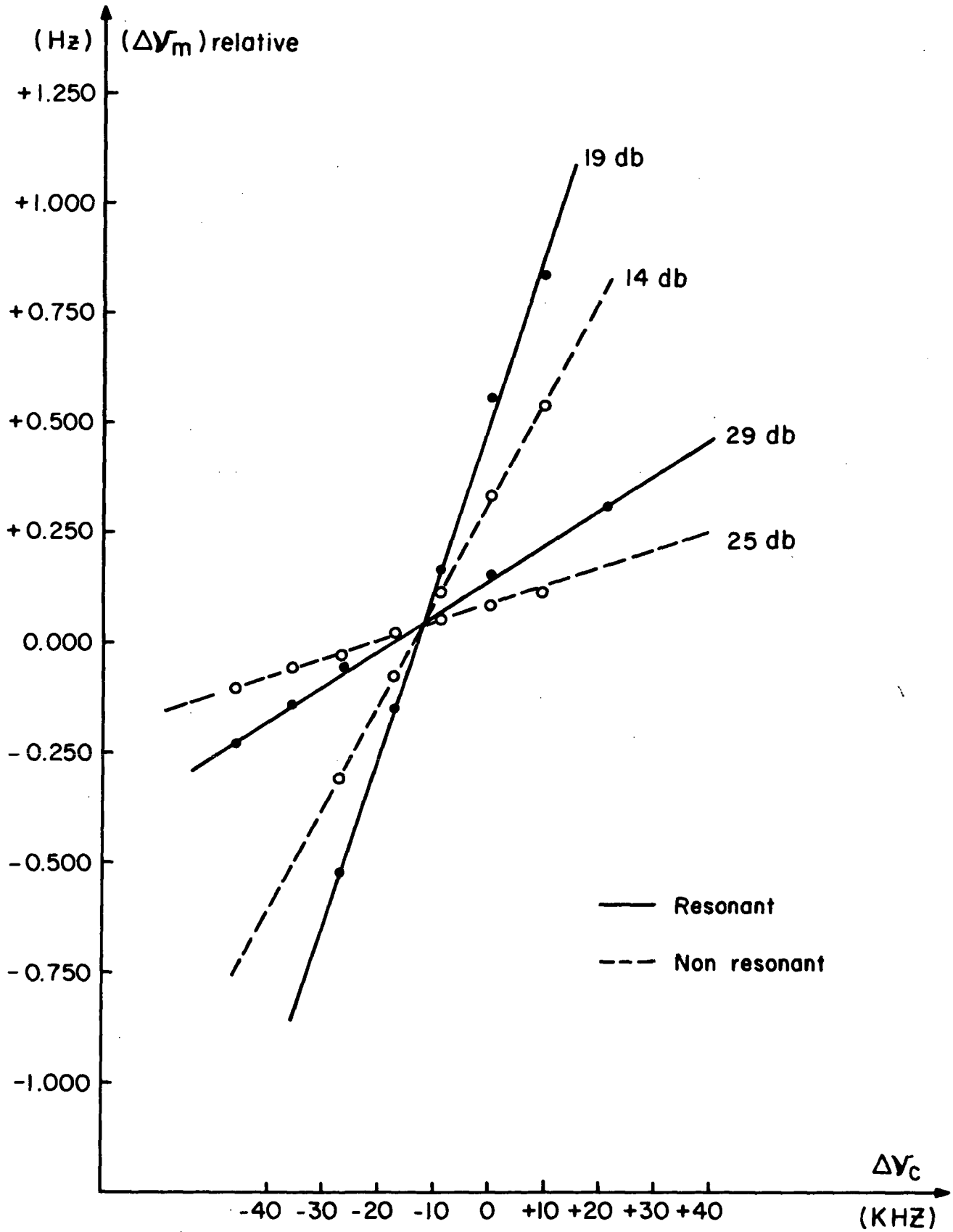
(Hz)
(ΔVm) relative
+1.250
+1.000
+0.750
+0.500
+0.250
0.000
-0.250
-0.500
-0.750
-1.000
19 db
14 db
29 db
25 db
Resonant
Non resonant
ΔVc
-40 -30 -20 -10 0 +10 +20 +30 +40
(KHZ)

Figure 14

EXPERIMENTAL SETUP

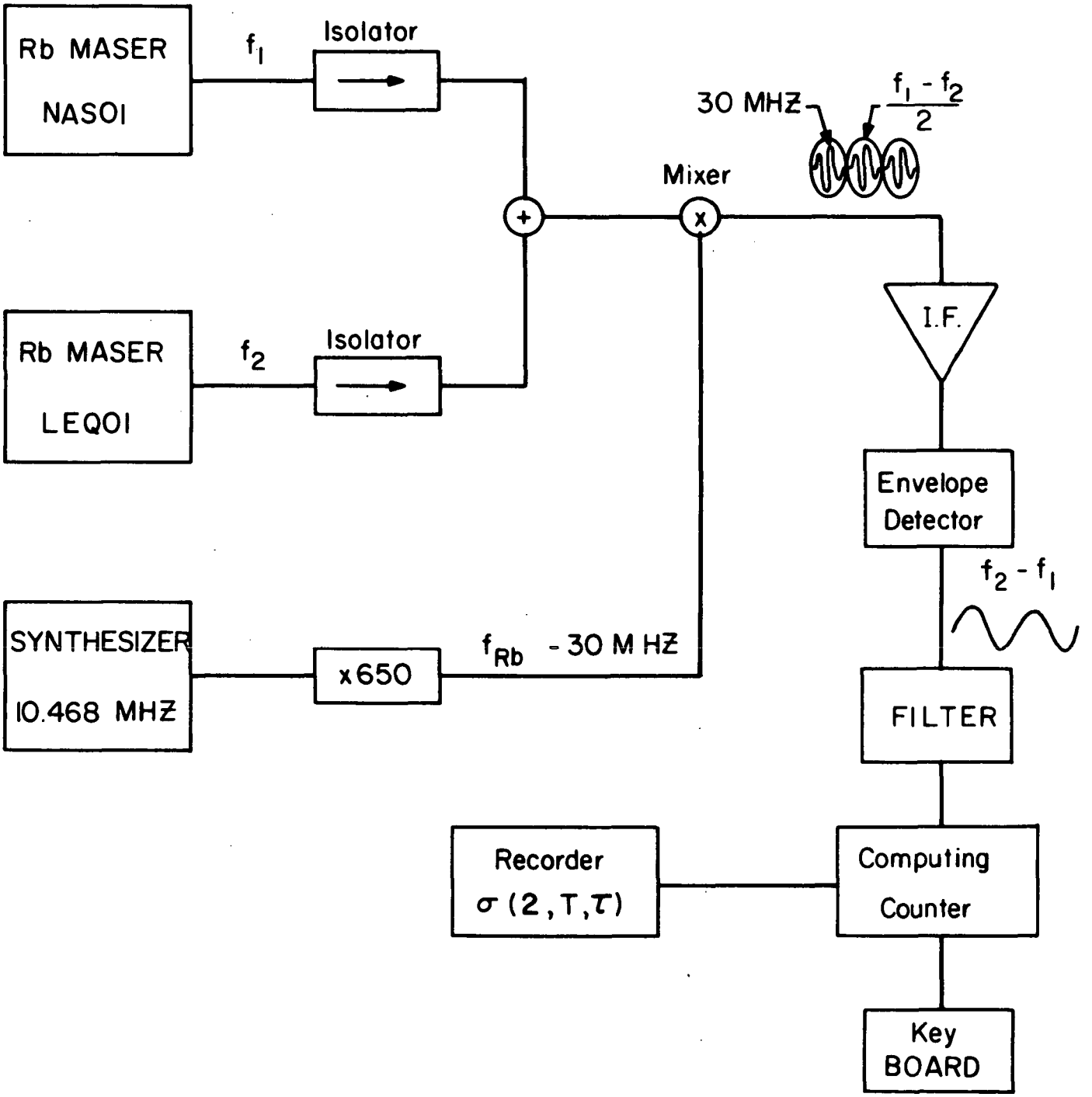

Figure 15

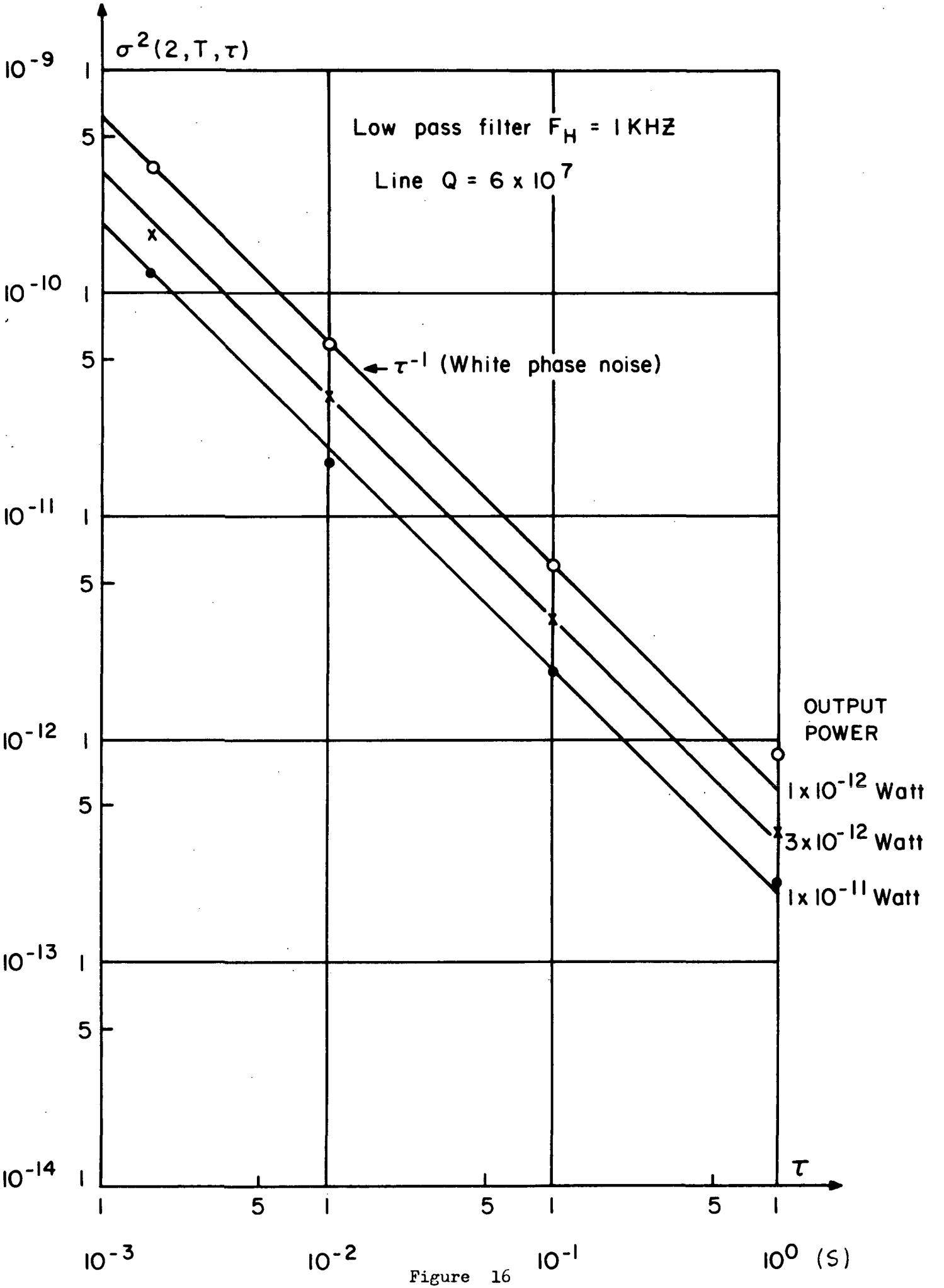
$\sigma^2(2,T,\tau)$
Low pass filter F_H = 1 KHz
Line Q = 6×10^7
τ^{-1} (White phase noise)
OUTPUT POWER
1×10^{-12} Watt
3×10^{-12} Watt
1×10^{-11} Watt
10^{-9}
10^{-10}
10^{-11}
10^{-12}
10^{-13}
10^{-14}
1
5
10^{-3}
10^{-2}
10^{-1}
10^{0} (S)
τ

Figure 16

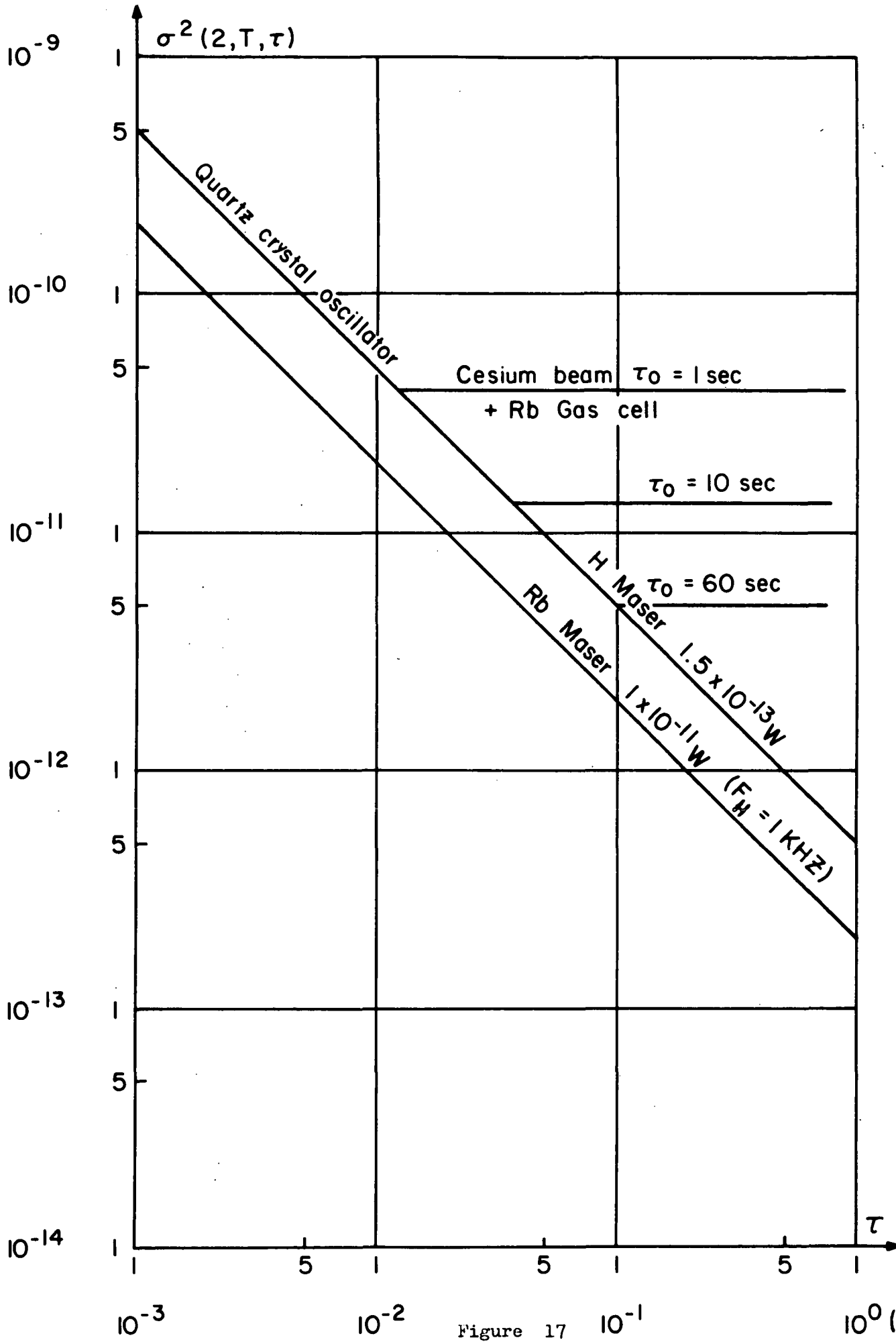
$\sigma^2(2,T,\tau)$
10^{-9}
10^{-10}
10^{-11}
10^{-12}
10^{-13}
10^{-14}
1
5
Quartz crystal oscillator
Cesium beam τ_0 = 1 sec
+ Rb Gas cell
τ_0 = 10 sec
τ_0 = 60 sec
H Maser 1.5 x 10^{-13} W
Rb Maser 1 x 10^{-11} W
(F_H = 1 KHZ)
τ
10^{-3}
10^{-2}
10^{-1}
10^{0} (S)

Figure 17

Figure 18